International Journal of Nanomedicine

Dovepress
Taylor & Francis Group

Open Access Full Text Article

ORIGINAL RESEARCH

Optimized Lipid Nanoparticle-Mediated mRNA Co-Delivery of SOX5/SOX9 Enables Synergistic Senescence Reversal for Osteoarthritis Therapy

Yang Yu[1,*], Zhongyin Ji[1,*], Hongjun Xu[1], Mingyang Ma[1], Shanni Li[1], Zhaojing Yin[2], Yiyang Du[2], Hui Li[3], Sen Liu[1], Wenwei Qian[1]

[1]Department of Orthopedic Surgery, Peking Union Medical College Hospital, Chinese Academy of Medical Sciences and Peking Union Medical College, Beijing, 100730, People's Republic of China; [2]School of Medicine, Tsinghua University, Beijing, 100084, People's Republic of China; [3]BiosynRNA Biotechnology Company, Beijing, 100190, People's Republic of China

*These authors contributed equally to this work

Correspondence: Sen Liu; Wenwei Qian, Department of Orthopedic Surgery, Peking Union Medical College Hospital, Chinese Academy of Medical Sciences and Peking Union Medical College, Beijing, 100730, People's Republic of China, Email liusen@pumch.cn; qianww@pumch.cn

Background: Chondrocyte senescence significantly impairs extracellular matrix (ECM) synthesis and accelerates cartilage degradation, driving osteoarthritis (OA) progression. Although gene therapies targeting senescent chondrocytes are promising for OA, developing strategies that simultaneously rejuvenate cartilage function and precisely modulate the inflammatory microenvironment remains challenging.

Methods: We developed an optimized lipid nanoparticle (LNP)-based delivery platform for the efficient co-delivery of transcription factors SOX5 and SOX9 mRNAs into chondrocytes. The physicochemical properties and biosafety of the formulations were systematically characterized. Additionally, the therapeutic efficacy of these formulations was evaluated in senescent chondrocyte cultures and an ACLT-induced osteoarthritis (OA) rat model.

Results: The synergistic action of SOX5 and SOX9 markedly enhanced anabolic signaling, promoting synthesis of critical cartilage ECM components (type II collagen and aggrecan). The combination also reduced inflammation-mediated matrix degradation in vitro and in vivo. In a rat OA model, this optimized LNP-mediated co-delivery substantially improved cartilage regeneration, suppressed joint inflammation, and restored joint function compared to single-gene treatment or untreated controls.

Conclusion: This work provides an advanced, synergistic mRNA therapeutic approach employing optimized LNPs to alleviate chondrocyte senescence and stimulate cartilage regeneration, representing a promising strategy for OA intervention.

Keywords: osteoarthritis, articular cartilage, lipid nanoparticles, senescence, mRNA delivery

Introduction

Osteoarthritis (OA), a prevalent degenerative joint disorder, affects over 300 million people worldwide and is a primary cause of chronic disability in the elderly.[1–5] Clinically characterized by persistent joint pain, stiffness, and progressive loss of mobility, OA pathologically involves articular cartilage degradation, subchondral bone sclerosis, osteophyte formation, and synovial inflammation.[6–8] With the increasing prevalence of aging and obesity, the economic burden of OA is escalating. Current therapies primarily provide symptomatic relief without halting disease progression, and OA-related healthcare expenditures in the United States alone are projected to exceed $100 billion annually by 2040.[9–12] Although total joint arthroplasty, specifically knee replacement, is still considered the best treatment for end-stage OA, its invasiveness, high cost, and limited long-term effectiveness make it a less than ideal choice. This is especially true considering the growing number of younger OA patients.[13–15] While pharmacological and intra-articular interventions—such as nonsteroidal anti-inflammatory drugs (NSAIDs), corticosteroids, hyaluronic acid, and platelet-rich plasma (PRP)—provide temporary symptomatic relief, these modalities fail to halt or reverse underlying cartilage degeneration.[16–18]

Received: 1 June 2025
Accepted: 30 September 2025
Published: 22 October 2025

Graphical Abstract

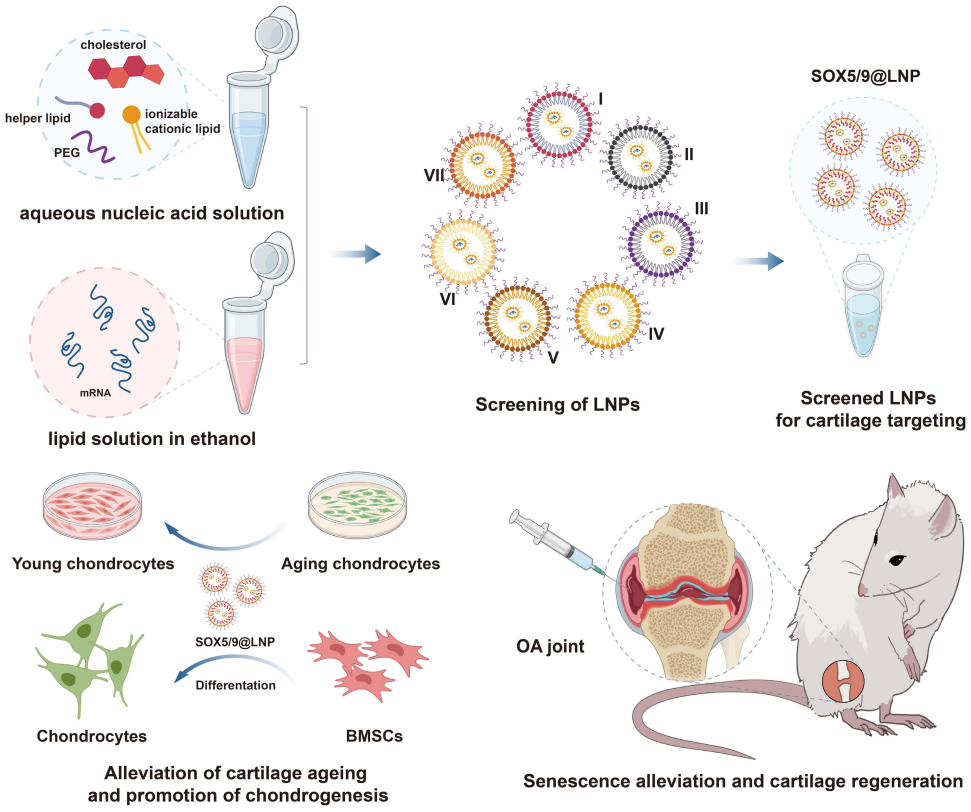

Similar concerns have been raised in recent high-impact studies that emphasize the lack of disease-modifying efficacy among currently available interventions.[3] To address these limitations, recent research has delved into sophisticated biomaterial- and nanotechnology-driven strategies. These encompass hydrogel/organoid constructs mimicking cartilage microenvironments and bone-targeted nanoparticles that modulate subchondral remodeling.[19,20] Although these approaches reflect a growing emphasis on disease-modifying and regenerative interventions, truly effective and clinically translatable therapies that directly address the root mechanisms of OA progression remain urgently needed.[21,22]

Cellular senescence has emerged as a critical factor underlying the development and progression of osteoarthritis. Senescent chondrocytes, which accumulate with aging, exhibit hallmark features including elevated senescence-associated β-galactosidase (SA-β-Gal) activity, increased expression of cell cycle inhibitors (p16-INK4A, p21-CDKN1A), and the secretion of inflammatory cytokines (IL-6, IL-8) and matrix-degrading enzymes (MMP-13, ADAMTS-5) through the senescence-associated secretory phenotype (SASP).[21,23–28] These senescent cells compromise the extracellular matrix (ECM) synthesis and integrity. They also propagate tissue degeneration via paracrine signaling, which adversely affects neighboring healthy chondrocytes and accelerates overall joint deterioration.[25,28] Therefore, the selective targeting and functional rejuvenation of senescent chondrocytes constitutes a promising therapeutic approach for restoring cartilage homeostasis and structural integrity in osteoarthritis.

Recent breakthroughs in mRNA-based therapeutics have revolutionized gene modulation therapies. This is exemplified by the rapid clinical success of mRNA vaccines for COVID-19.[29–31] Compared to traditional DNA-based gene delivery methods, mRNA therapeutics offer key advantages including transient and dose-controllable protein expression without the risk of genomic integration.[29,31–34] Despite its therapeutic promise, mRNA delivery remains technically challenging due to rapid enzymatic degradation, limited intracellular uptake, and potential immunogenicity.[35] To address these barriers, lipid nanoparticles (LNPs) have emerged as the leading platform for nucleic acid delivery, effectively

encapsulating and protecting mRNA payloads, enhancing cellular internalization, and promoting efficient cytoplasmic release.[36–39] Leveraging their ability to penetrate dense, avascular tissues like cartilage, optimized LNP formulations hold immense promise for the targeted, localized treatment of OA.

In cartilage biology, the transcription factor SOX9 plays a central role by orchestrating the expression of key ECM components such as type II collagen (COL II) and aggrecan (ACAN).[40–42] SOX9 is indispensable for mesenchymal stem cell commitment to the chondrogenic lineage, as evidenced by severe cartilage malformations upon SOX9 deficiency in both human genetic disorders and animal models.[43–45] Importantly, the transcriptional activity of SOX9 is greatly amplified by the co-expression of SOX5 and SOX6, which together form the so-called "SOX trio".[46] Although SOX5 and SOX6 lack intrinsic transactivation domains, they synergize with SOX9 at cartilage-specific enhancers, enhancing gene transcription and stabilizing the chondrocyte phenotype.[47–49] Emerging evidence indicates that SOX5 may independently promote cellular rejuvenation. For example, a genome-wide CRISPR activation screen identified SOX5 as a top candidate for reversing cellular senescence in human mesenchymal precursor cells by reactivating pro-regenerative genes such as HMGB2.[50] Furthermore, intra-articular delivery of SOX5 in aged OA mouse models mitigated cartilage degeneration and improved joint histology, achieving regenerative effects comparable to Yamanaka factor-based reprogramming, but without altering cellular identity. These findings strongly support the rationale for co-delivering SOX5 and SOX9 to osteoarthritic joints. While SOX9 re-establishes core cartilage matrix synthesis, SOX5 not only enhances SOX9's transcriptional efficacy but may also directly reverse senescence-associated impairments.

In this study, we developed an optimized LNP-mediated mRNA delivery strategy designed specifically to co-deliver SOX5 and SOX9 into chondrocytes (Scheme 1). Through systematic formulation screening, we identified the most efficient LNP composition. It is capable of targeting chondrocytes, maximizing intracellular mRNA delivery, and enhancing gene expression in both in vitro and in vivo contexts. In a surgically induced rat OA model, we further validated the therapeutic efficacy of our dual-mRNA delivery system, demonstrating significant improvements in cartilage ECM restoration, reduced joint inflammation, and enhanced functional recovery compared to single-factor controls and untreated animals. Collectively, this work establishes an innovative, mechanism-driven nanotherapeutic approach. It leverages optimized LNP technology and transcription factor co-delivery to effectively target chondrocyte senescence and promote cartilage regeneration in osteoarthritis.

Materials and Methods

Materials and Reagents

DMG-PEG 2000, SM-102, 1,2-Distearoyl-sn-glycero-3-phosphorylcholine and Cholesterol was purchased from Medchemexpress Inc. (Shanghai, China). Different ratios of LNPs (SM-102) were synthesised and supplied by Biosyn (Beijing) Biotechnology Co. Calcein/PI Cell Viability/Cytotoxicity Assay Kit and SA-β-Gal staining kit were from Beyotime Biotechnology Co., Ltd. (Shanghai, China). Cell Counting Kit-8 (CCK-8) was obtained from Biosharp (Anhui, China). Radio-immunoprecipitation assay (RIPA) buffer and 2-(4-Amidinophenyl)-6-indolecarbamidine dihydrochloride (DAPI) were from Beyotime Institute of Biotechnology (Shanghai, China). Hydrogen peroxide (H_2O_2) was purchased from Sigma-Aldrich Trading Co., Ltd. (Shanghai, China). Anti-Collagen II antibody (#ab307674) and anti-SOX9 antibody (#ab185230) were obtained from Abcam Inc. (Cambridge, MA, USA). CDKN2A/p16INK4a Rabbit mAb (A11651), CDKN1A/p21 Rabbit mAb (A19094), GAPDH antibody (A19056), Anti-Aggrecan antibody (A11691) and Anti-SOX5 antibody (A23127) were from ABclonal Biotechnology Co., Ltd. (Wuhan, China). CoraLite488-conjugated Goat Anti-Rabbit IgG (H+L) and CoraLite594 – conjugated Goat Anti-Rabbit IgG (H+L) was purchased from Proteintech (Wuhan, China). Fetal bovine serum (FBS), phosphate buffered saline (PBS) and dulbecco's modified eagle medium nutrient mixture F-12 (DMEM/F-12) were provided by Gibco. Paraformaldehyde and ELISA kits (TNF-α, IL-1β, and IL-6) were purchased from Wuhan servicebio technology CO., Ltd. (Wuhan, China). JC-1 assay kit and paraformaldehyde (4%), and Triton X-100 (0.1%) were purchased from Beyotime Biotechnology. (Shanghai, China). Dio were from UElandy Inc. (Soochow, China). Deionized (DI) water with a resistivity of 18.2 Ω was used throughout this project.

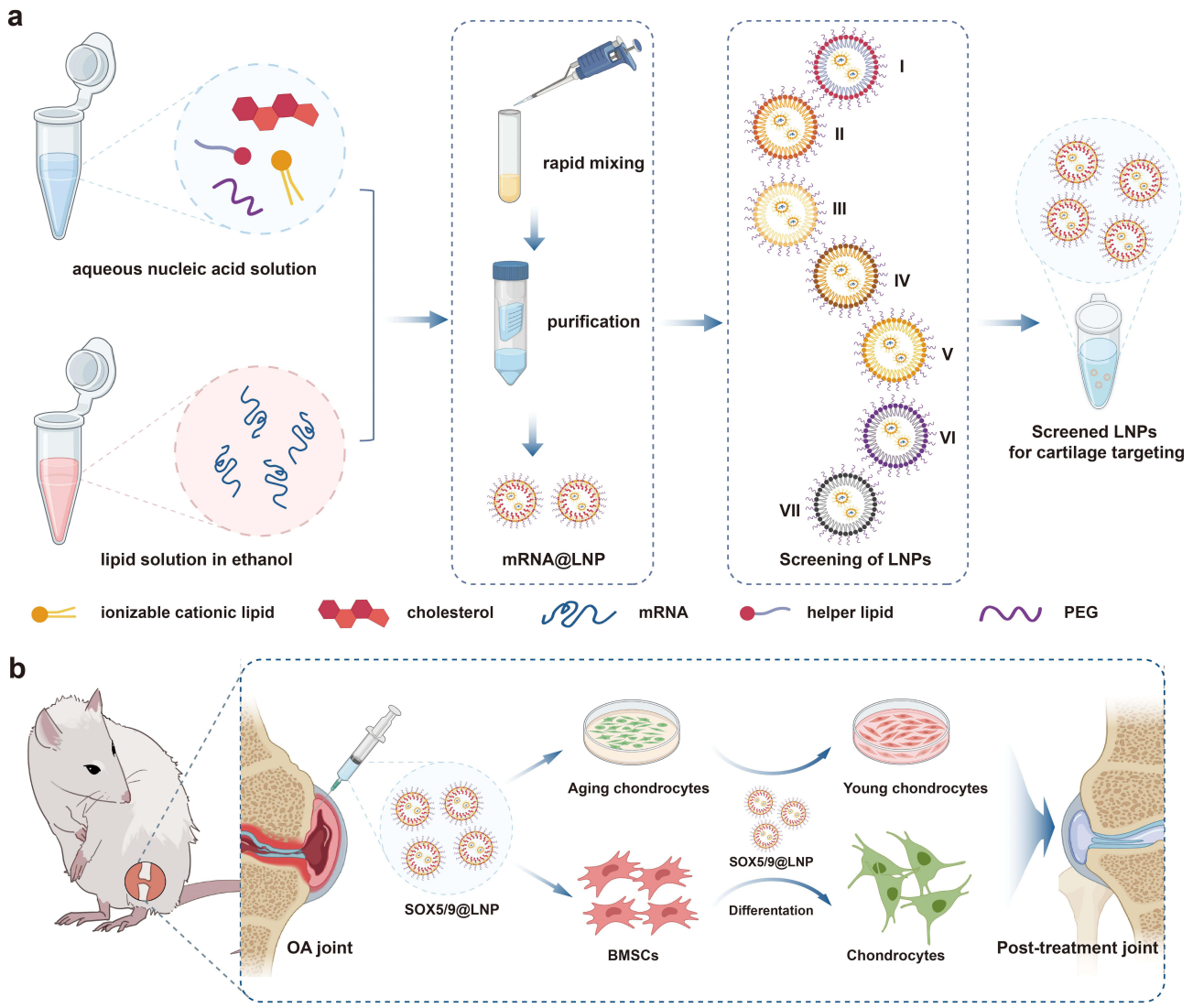

Scheme 1 Schematic illustration of the synthesis and therapeutic performance of SOX5/9@LNPs. (**a**) Preparation and optimization of seven distinct LNP formulations. (**b**) In vitro and in vivo evaluation of their efficacy in reversing chondrocyte senescence and promoting cartilage regeneration.

Characterization

Seven lipid nanoparticle (LNP) formulations were systematically designed by varying the molar ratios of four components: SM-102 (ionizable lipid), cholesterol, DSPC, and DMG-PEG2000, with SM-102 serving as the primary lipid. The molar ratios of SM-102 ranged from 40% to 60%, while cholesterol, DSPC, and DMG-PEG2000 were adjusted accordingly to generate distinct compositions. Specifically, Formulation I–VII included combinations such as SM-102: 50–60%, Cholesterol: 28.5–48.5%, DSPC: 10–15%, and DMG-PEG2000: 1.5–2.0%. All lipids were dissolved in ethanol and mixed with luciferase mRNA dissolved in citrate buffer (pH 4.0) using a microfluidic mixing technique to obtain uniform mRNA-loaded LNPs. The resulting formulations were purified by dialysis and filtered through 0.22 μm membranes. The physicochemical characteristics of the formulated LNPs were subsequently evaluated as follows. Transmission electron microscopy (TEM) images were conducted on a JEM-2100F transmission electron microscope at an acceleration voltage of 200 kV. Dynamic Light Scattering (DLS), zeta potential examinations and polydispersity index (PDI) were obtained from the Malvern Nano-ZS90 Zetesizer (Malvern Instrument Ltd., US). Luciferase mRNA-loaded LNPs (Luciferase@LNPs) were evaluated for intracellular expression efficiency in chondrocytes by measuring luminescence intensity with a microplate reader (Biotek SynergyNeo2, USA), which reflected the successful delivery and

translation of luciferase mRNA. Confocal laser scanning microscopy (CLSM) images were captured by high speed confocal platform (Andor, UK). Tissue sections were observed by Olympus VS120 (Olympus Company, Japan).

Cell Culture

Primary articular chondrocytes and bone marrow-derived mesenchymal stem cells (BMSCs) were isolated from 2-week-old Sprague–Dawley (SD) rats (purchased from Vital River Laboratory Animal Technology in Beijing) following standard protocols. Briefly, femoral head cartilage was aseptically dissected and washed three times with sterile phosphate-buffered saline (PBS). The tissue was minced into ~1 mm^3 fragments and sequentially digested with 0.25% trypsin at 37 °C for 30 min, followed by overnight incubation with 0.025% type II collagenase to release chondrocytes. Isolated primary chondrocytes were cultured in high-glucose Dulbecco's Modified Eagle Medium (DMEM) supplemented with 10% fetal bovine serum (FBS) and 1% penicillin–streptomycin. For BMSC isolation, femurs and tibiae were harvested from euthanized SD rats. After removing both epiphyses, bone marrow was flushed out with complete medium until the bones turned pale. The collected marrow suspension was cultured in low-glucose DMEM with 10% FBS and 1% penicillin–streptomycin. Non-adherent cells were removed by changing the medium every 24 h to enrich for adherent BMSCs. All cells were maintained at 37 °C in a humidified atmosphere containing 5% CO_2.

In vitro Evaluation of Luciferase mRNA–LNP Expression in Chondrocytes

To assess the transfection efficiency of different LNP formulations in vitro, chondrocytes were seeded into 96-well plates at a density of 1×10^4 cells per well and allowed to adhere overnight. Seven distinct luciferase mRNA–LNP formulations (designated as I~VII) with varying SM-102 compositions were added to the cells and incubated for 12 h under standard culture conditions. Following treatment, luciferase expression levels were quantified using a microplate reader (Biotek SynergyNeo2, US) according to the instructions of the luciferase assay kit. Luminescence intensity was recorded and compared to evaluate the transfection efficiency of each LNP formulation.

In vivo Bioluminescence Imaging of Luciferase mRNA–LNP Expression

All animal procedures were conducted using 8-week-old male Sprague–Dawley (SD) rats. To assess in vivo protein expression of mRNA–LNP formulations, the three luciferase mRNA–LNPs (formulations I, II, and IV) showing the highest expression in vitro in chondrocytes were selected for further evaluation. Each formulation was administered via a single intra-articular injection into the knee joint. At 12 and 24 h post-injection, in vivo luciferase expression was monitored using an IVIS Spectrum imaging system (PerkinElmer, USA). Bioluminescence signals were acquired and quantified to compare the relative transfection efficiency of the different LNP formulations.

Senescence-Associated β-Galactosidase SA-β-Gal Staining

Senescence in chondrocytes was assessed using a commercial SA-β-Gal staining kit (Beyotime, C0602) according to the manufacturer's instructions. Chondrocytes were seeded into 24-well plates and fixed with 0.2% glutaraldehyde for 10 min at room temperature. After washing, cells were incubated overnight at 37 °C in X-gal staining solution (pH 6.0) to detect β-galactosidase activity. Images of stained cells were captured using an Olympus light microscope. The percentage of SA-β-Gal-positive cells was quantified from at least five randomly selected fields per sample. Data are presented as mean ± SD from three independent experiments (n = 3).

In vitro Cytotoxicity Evaluation

The chondrocytes / rBMSCs were incubated with mRNA@LNP at gradient concentrations (0, 0.01, 0.05, 0.1, 0.5 and 1 μg mL^{-1}) for 24 h. Cell viability was tested by microplate reader (Infinite m nano 2022657S, Tecan spark) using the Cell Counting Kit-8 (CCK8) assay. Cell viability was calculated according to the Equation (1):

$$\text{Cell viability } (\%) = \frac{C - A}{C} 100\% \quad (1)$$

 https://doi.org/10.2147/IJN.S544168

where A represents the optical density (OD) at 450 nm of cell with LNPs at different concentrations co-incubation, and C represents OD values of cells treated without LNPs. For live/dead staining assay, rBMSCs were cultured in confocal dishes and incubated with LNPs at different concentrations (0, 0.01, 0.05, 0.1, 0.5 and 1 μg mL^{-1}) separately after washed with PBS for two times. Next, the dishes were placed in the cell incubator for another 6 h. Then the cells were stained with Calcein-AM/PI for 20 min before washed with PBS for two times. The ultimate images were observed through CLSM.

To further assess potential immunotoxicity, rat bone marrow–derived macrophages (BMDMs) were isolated from femurs and tibias of Sprague–Dawley rats and cultured in DMEM supplemented with 10% FBS and 1% penicillin–streptomycin. Cells were seeded into 96-well plates at a density of 1×10^4 cells per well and allowed to adhere overnight. BMDMs were then incubated with LNPs (control group, SOX5@LNP, SOX9@LNP and SOX5/9@LNP) at a concentration equivalent to 1 μg·mL^{-1} mRNA for 24 h, while untreated cells served as the control. Cell viability was determined using the CCK-8 assay following the manufacturer's protocol. Briefly, 10 μL of CCK-8 solution was added into each well, incubated for 2 h at 37 °C, and absorbance was measured at 450 nm with a microplate reader. For cytokine secretion analysis, culture supernatants were collected after 24 h of treatment, centrifuged at 1500 rpm for 10 min to remove debris, and stored at −80 °C until use. ELISA kits were used to quantify TNF-α, IL-1β, and IL-6 levels. Briefly, 100 μL of standards or samples was added to pre-coated wells, incubated for 2 h, followed by sequential incubation with biotinylated antibodies and HRP-conjugated streptavidin. After TMB substrate reaction, absorbance was measured at 450 nm using a microplate reader. Cytokine concentrations were calculated from standard curves and expressed as pg·mL^{-1}.

Intracellular ROS Dictation

Chondrocytes (1.0×10^4 cells per well) were seeded onto confocal dishes and incubated for 24 h. After washing twice with PBS, cells were subjected to the following treatments: (1) control group, (2) SOX5@LNP, (3) SOX9@LNP, (4) SOX5/9@LNP. After 4 h of treatment, cells were washed twice with PBS and incubated with DCFH-DA working solution for 30 min to assess intracellular reactive oxygen species (ROS) levels. Following staining, cells were washed again with PBS and visualized under a confocal laser scanning microscope (CLSM). For flow cytometry analysis, chondrocytes were seeded in 6-well plates and treated using the same procedure described above. Fluorescence intensity was measured using a spectrophotometer.

Real-Time Quantitative Polymerase Chain Reaction RT-qPCR Analysis

The mRNA expression levels of target genes were evaluated by real-time quantitative reverse transcription polymerase chain reaction (RT-qPCR). To assess gene expression changes in chondrocytes under different treatments, the expression levels of key cartilage-related markers and senescence-associated genes—including collagen type II (COL II), aggrecan (ACAN), and the cell cycle inhibitor p21—were analyzed. Chondrocytes were subjected to one of the following treatments for 7 days: (1) control, (2) SOX5@LNP, (3) SOX9@LNP, or (4) SOX5/9@LNP. Total RNA was extracted using TRIzol reagent (Invitrogen, USA), and purified RNA was reverse-transcribed into complementary DNA (cDNA) using the PrimeScript™ RT Master Mix (Takara, Japan) according to the manufacturer's protocol. RT-qPCR was performed using the StepOnePlus™ Real-Time PCR System (Applied Biosystems, USA) and the SYBR Green RT-PCR kit (Takara, Japan) to quantify the expression levels of target genes. Each reaction was carried out in triplicate, and relative gene expression was calculated using the $2^{-\Delta\Delta cT}$ method.

Western Blot Analysis

Chondrocytes subjected to different treatments (0, 0.01, 0.05, 0.1, 0.5 and 1 μg mL^{-1}) for 1, 4, and 7 days were harvested on ice and washed twice with ice-cold phosphate-buffered saline (PBS). Total protein was extracted using RIPA lysis buffer supplemented with protease inhibitors, followed by incubation on ice for 30 min. Lysates were clarified by centrifugation at 10,000 rpm for 10 min at 4 °C, and protein concentrations were quantified using a BCA protein assay kit. Equal amounts of protein were mixed with loading buffer, denatured, and separated by 10% sodium dodecyl sulfate-polyacrylamide gel electrophoresis (SDS-PAGE), then transferred onto polyvinylidene difluoride (PVDF) membranes.

Membranes were blocked in 5% non-fat dry milk in Tris-buffered saline with 0.1% Tween-20 (TBST) for 1 h at room temperature, followed by incubation with primary antibodies overnight at 4 °C. The primary antibodies used were as follows: anti-GAPDH (1:1000), anti-SOX9 (1:1000), anti-SOX5 (1:1000), anti-collagen type II (COL II, 1:1000), and anti-p21 (1:1000). After three washes with TBST, membranes were incubated with appropriate secondary antibodies for 1 h at room temperature. The PVDF membranes were then washed three times with Tris-buffered saline containing 0.1% Tween-20 (TBST) and incubated with the appropriate secondary antibodies for 1 h at room temperature. Finally, protein bands were visualized using an enhanced chemiluminescence (ECL) detection kit (Solarbio, China). Protein bands were visualized using a chemiluminescence imaging system (MiniChemi610, Beijing, China). GAPDH was used as an internal control to ensure equal protein loading across samples.

Scratch Test

Senescent chondrocytes were seeded into 6-well Transwell plates (Corning, USA) and cultured to full confluence. A sterile 200 μL pipette tip was used to create a linear scratch across the cell monolayer. After scratching, the cells were washed to remove debris and incubated in serum-free medium under different treatment conditions: (1) control, (2) SOX5@LNP, (3) SOX9@LNP, and (4) SOX5/9@LNP. Images of chondrocyte migration were captured at 0 and 24 h using a phase-contrast microscope. The wound area was measured at each time point, and the migration rate was calculated using the following formula: Migration rate (%) = $(A_0 - A_n) / A_0 \times 100\%$, where A_0 represents the initial scratch area at 0 h and A_n represents the remaining scratch area at the indicated time point.

Fluorescence Imaging of Chondrocytes and rBMSCs

Chondrocytes/rBMSCs (1.0×10^4 cells per well) were cultured in 24-well plates and fixed with 4% paraformaldehyde for 15 min. After fixation, cells were washed three times with PBS and permeabilized using 0.2% Triton X-100 in PBS for 15 min. Non-specific binding was blocked with 5% bovine serum albumin (BSA) for 30 min at room temperature. Cells were then incubated overnight at 4 °C with primary antibodies against collagen type II (COL II), aggrecan (ACAN), P16 and P21. After washing, fluorescently labeled secondary antibodies were applied for 1 h at room temperature. Nuclei were counterstained with DAPI, and fluorescence images were acquired using a confocal laser scanning microscope (CLSM).

In vivo Biocompatibility Evaluation

Twenty SD rats (8 weeks old, male, 200 g in weight) were bought from Vital River Laboratory Animal Technology in Beijing. All experimental protocols were approved by the Ethics Committee on animal experiments of the National Center for Nanoscience and Technology (Approval number: NCNST21-2312-0602) and conducted in strict compliance with China's national standard GB/T 35892–2018 (Guidelines for Ethical Review of Laboratory Animal Welfare) as well as the ARRIVE guidelines. Twenty rats were randomly divided into four groups: the control group was administrated with 100 μL of physiological saline through tail vein injection and the other group was treated with 100 μL of SOX5@LNPs, SOX9@LNPs and SOX5/9@LNPs for 7 days of observation. After 7 days, the rats were euthanized and major tissues (heart, liver, spleen, lung and kidney) along with blood samples were obtained for subsequent H&E staining for pathological evaluation. Blood routine and biochemical tests (RBC, MCH, HGB, MCHC, MCV, HCT, PLT, WBC, Lymph, Mon, Gran, ALT, AST, ALP, BUN, and CREA) were carried out through automatic blood cell analyzers (BC-2800vet, Maydeal and Chemray 240, Rayto).

In vivo OA Model with mRNA-LNP Infection

The Sprague Dawley rats (6 weeks old, male, 200 g in weight) were provided by Beijing Vital River Laboratory Animal Technology Co., Ltd. To investigate the therapeutic effects of SOX5/9@LNP in osteoarthritis (OA), an anterior cruciate ligament transection (ACLT) model was established in Sprague–Dawley (SD) rats to induce knee joint OA. The construction of OA model was confirmed through 3D micro-CT in the pre-experiment (Figure S7). Rats were randomly assigned into five groups: normal group, OA model control group, SOX5@LNP group, SOX9@LNP group, and SOX5/9@LNP group. Under isoflurane anesthesia, the right anterior cruciate ligament was carefully exposed and transected under direct vision in all groups except the normal group. Two weeks after surgery, intra-articular injections were performed based on group assignments. Rats

in the SOX5@LNP, SOX9@LNP, and SOX5/9@LNP groups received the corresponding formulations via intra-articular injection twice per week for two consecutive weeks. Control and normal groups received equivalent volumes of physiological saline at the same time points. To assess the effectiveness of the treatment, five groups of rats were sacrificed at the fourth and eighth postoperative weeks respectively, and the femur was removed to observe the condition of the bone tissue under micro-CT (SCANCO, Switzerland) and the bone tissue was excised for further histological analysis with H&E, Masson, SO/FG, Toluidine Blue and COL II. In addition, the major organs (heart, liver, spleen, lung, and kidney) were collected for H&E staining evaluation (Figures S13 and S14). Images of tissue slices were captured by the panoramic digital section scanning microscope Olympus VS120 (Olympus Company, Japan).

Transcriptome Sequencing

Senescent rat chondrocytes were treated with SOX5/9@LNP or left untreated (control group) for transcriptomic comparison. Total RNA was extracted using TRIzol reagent (Invitrogen, USA) and quantified with NanoDrop 2000 (Thermo Fisher Scientific). RNA integrity was assessed using the Agilent 2100 Bioanalyzer (Agilent Technologies, USA), and samples with RIN $\geq$ 7.0 were selected for further processing. RNA sequencing was performed by technical staff at Beijing Qingke Biotechnology Co., Ltd. Sequencing was carried out on an Illumina NovaSeq 6000® platform (Illumina Inc., USA) with paired-end 150 bp reads. Raw reads were filtered and trimmed using fastp (https://github.com/OpenGene/fastp), and clean reads were aligned to the Rattus norvegicus reference genome (mRatBN7.2) using HISAT2. Transcript abundance was estimated with StringTie (https://github.com/gpertea/stringtie). Genes with |log2 fold change| $\geq$ 1 and adjusted p-value (FDR) < 0.05 were considered differentially expressed genes (DEGs). Functional enrichment analysis, including Gene Ontology (GO) and KEGG pathway enrichment, was performed using the clusterProfiler package in R.

Statistical Analysis

All experimental data are presented as mean ± standard deviation (SD) from at least three independent replicates. Statistical significance was evaluated using two-tailed Student's t-tests or two-way analysis of variance (ANOVA), as appropriate, performed with GraphPad Prism 9.3 (GraphPad Software Inc., USA). The tests were regarded as statistically significant with signs of *p < 0.05, **p < 0.01, and ***p < 0.001.

Results and Discussion

LNP Formulation and Characterization

To establish an efficient mRNA delivery platform tailored for chondrocytes, a panel of seven lipid nanoparticle (LNP) formulations (I–VII) based on SM-102 were systematically designed and evaluated. These LNPs were thoroughly characterized with respect to their morphology, size distribution, surface charge, colloidal stability, and transfection capacity in chondrocytes. Transmission electron microscopy (TEM) revealed that all LNPs exhibited uniform spherical morphology with smooth surfaces and monodisperse appearance. This indicates favorable structural integrity and suitability for cellular uptake (Figures 1a and b, S1 in the ESM). This morphology is known to enhance endocytosis, particularly in non-phagocytic cells such as chondrocytes, where particle shape and uniformity significantly influence uptake dynamics.[51,52] Dynamic light scattering (DLS) analysis revealed that the hydrodynamic diameters of all seven LNP formulations ranged between 100 and 200 nm (Figures 1c and S2 in the ESM). This size range is optimal for clathrin- and caveolae-mediated endocytosis and additionally facilitates intra-cartilaginous diffusion.[53] Zeta potential analysis showed near-neutral surface charges across the formulations (Figure 1d), which is advantageous for minimizing nonspecific protein adsorption and prolonging circulation time by evading rapid clearance via the mononuclear phagocyte system. Furthermore, all LNPs exhibited low polydispersity index (PDI < 0.3) (Figure 1e), indicating narrow particle size distribution and excellent colloidal stability. A low PDI is crucial for ensuring consistent pharmacokinetics, cellular uptake, and reproducible biological responses—especially important in therapeutic applications where dosing precision is required. Collectively, these physicochemical characterizations confirmed that the synthesized LNPs possessed ideal properties for nucleic acid delivery, prompting further evaluation of their mRNA transfection performance in chondrocytes.

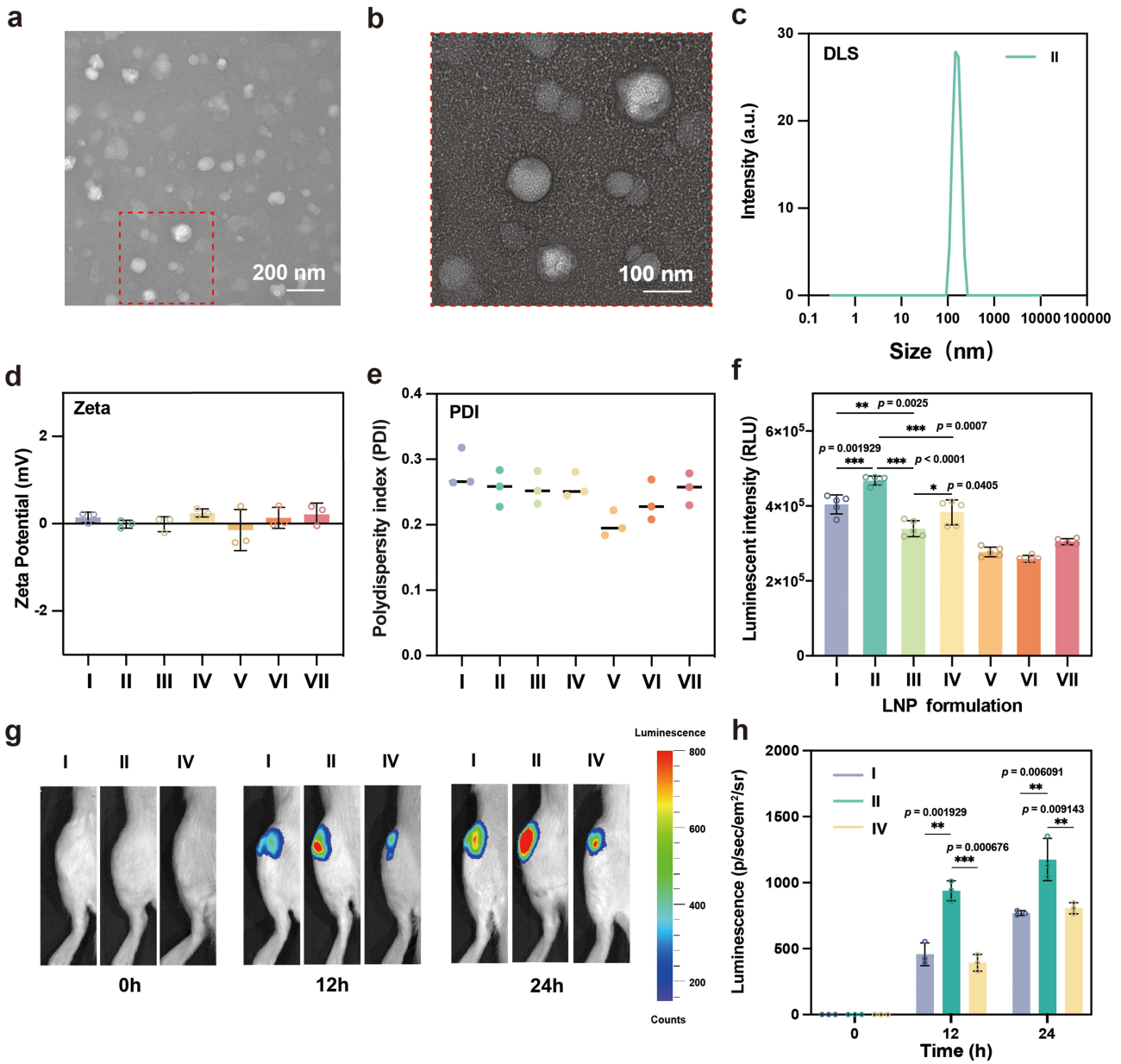

Figure 1 Physicochemical characterization of seven SM-102-based LNP formulations (I–VII). (**a** and **b**) Transmission electron microscopy (TEM) images of formulation II. (**c**) DLS results demonstrating the hydrodynamic size distribution of LNP formulation II. (**d**) Zeta potential measurements indicating near-neutral surface charges, favorable for biocompatibility. (**e**) PDI values for all formulations. (**f**) Luminescence intensity at 12 h post-transfection in primary chondrocytes treated with seven different luciferase mRNA-loaded LNP formulations (I–VII). (**g**) In vivo bioluminescence imaging of rat knee joints following intra-articular injection of formulations I, II, and IV, performed at 12 and 24 h post-injection. (**h**) Quantitative analysis of in vivo luminescence intensity demonstrated that formulation II yielded the highest signal, indicating superior delivery efficiency and joint retention (*$p < 0.05$, **$p < 0.01$, and ***$p < 0.001$).

In vitro and in vivo Luciferase mRNA LNP Delivery

To evaluate the mRNA delivery efficacy and joint-specific tropism of the SM-102-based LNP formulations, we encapsulated luciferase-encoding mRNA into seven candidate LNPs (formulations I–VII) and assessed their transfection efficiency using primary chondrocytes. Equal doses of mRNA were delivered to cultured chondrocytes in vitro, followed by quantification of intracellular luciferase activity after 12 h incubation. The resulting luminescence signals varied significantly among the different formulations, with formulations I, II, and IV exhibiting substantially elevated transgene expression (Figure 1f). Among them, formulation II showed the highest luminescence intensity, indicating its superior mRNA delivery efficiency in chondrocytes. These in vitro findings were consistent with the favorable physicochemical

https://doi.org/10.2147/IJN.S544168

characteristics of formulation II, including its optimal particle size, surface charge, and low polydispersity. To determine whether the superior transfection observed in vitro would translate to the in vivo joint environment, we next evaluated the three top-performing formulations (I, II, and IV) in a rat model. Each LNP was administered via a single intra-articular injection into the knee joints of SD rats, followed by in vivo bioluminescence imaging using an IVIS Spectrum system at 12 and 24 h post-injection. The imaging results demonstrated that all three formulations were able to deliver luciferase mRNA and mediate protein expression in vivo, but formulation II consistently yielded the strongest bioluminescence signal at both time points (Figure 1g and h). Notably, the expression from formulation II was not only the most intense but also showed more sustained signal retention over time, indicating enhanced intracellular delivery and expression efficiency within the joint cavity.

These findings collectively support formulation II (SM-102: 60%, Cholesterol: 28.5%, DSPC: 10%, DMG-PEG2000: 1.5%) as the optimal LNP composition for chondrocyte-targeted mRNA delivery. Its superior performance across both in vitro and in vivo contexts provides a compelling rationale for its use as the delivery vehicle in subsequent therapeutic experiments involving SOX5 and SOX9 mRNA co-delivery for cartilage regeneration.

Establishment and Validation of a Senescent Chondrocyte Model

To recapitulate the senescent phenotype observed in osteoarthritic cartilage, an in vitro model of chondrocyte senescence was established using hydrogen peroxide (H_2O_2)-induced oxidative stress. Primary rat chondrocytes were initially exposed to 40 μmol L^{-1} H_2O_2 for 24 h to induce acute oxidative injury, followed by sustained exposure to 10 μmol L^{-1} H_2O_2 for an additional 72 h to maintain the senescent state. Successful induction of senescence was confirmed by senescence-associated β-galactosidase (SA-β-Gal) staining, which revealed a substantial increase in SA-β-Gal–positive cells compared to untreated controls (Figure 2a and b). Concurrently, Western blot analysis demonstrated a pronounced decline in the expression of key chondrogenic markers (SOX5, SOX9, and COL II), accompanied by upregulation of the cell cycle inhibitor p21 (Figure 2c), a hallmark of senescence. Together, these results confirm the successful establishment of a senescent chondrocyte model, providing a reliable platform for subsequent evaluation of SOX5/9@LNP-mediated rejuvenation and cartilage regenerative therapies.

In vitro And in vivo Biocompatibility of the SOX5/9@LNPs

A thorough evaluation of the biocompatibility of SOX5/9@LNPs was conducted to ensure their safety for potential clinical translation. In vitro cytotoxicity was first assessed in primary rat articular chondrocytes and rat bone marrow-derived mesenchymal stem cells (rBMSCs). Cells were incubated with increasing concentrations of SOX5/9@LNPs (0, 0.01, 0.05, 0.1, 0.5, and 1 μg·mL^{-1}) for 24 h, and cell viability was measured using the Cell Counting Kit-8 (CCK-8) assay. Across all concentrations, SOX5/9@LNPs exhibited minimal cytotoxicity, maintaining cell viability above 90% even at the highest dose (Figures 2d and S3 in the ESM), indicating a broad therapeutic window and favorable dose tolerance.

To further visualize cellular responses, live/dead staining was performed using a Calcein-AM/PI Cell Viability/Cytotoxicity Assay Kit. Confocal microscopy imaging revealed a predominance of green fluorescence (Calcein-AM, viable cells) with minimal red fluorescence (PI, dead cells) in SOX5/9@LNP-treated chondrocytes, corroborating the high cell viability observed in the CCK-8 assay (Figure 2e). To further evaluate the immunotoxicity of the LNP formulations, we first incubated rat bone marrow–derived macrophages (BMDMs) with LNPs for 24 h. CCK-8 assay results showed no significant reduction in cell viability, indicating good in vitro biocompatibility (Figure S4a in the ESM). In addition, ELISA analysis revealed that the secretion levels of pro-inflammatory cytokines, including TNF-α, IL-1β, and IL-6, did not differ significantly between the groups treated with SOX5@LNP, SOX9@LNP, SOX5/9@LNP and the control group, indicating that LNPs did not elicit an inflammatory response (Figure S4b in the ESM). These results collectively demonstrate excellent in vitro cytocompatibility, supporting the safe application of SOX5/9@LNPs in cartilage-targeted gene delivery.

In vivo biosafety was further validated in Sprague–Dawley rats following systemic administration of SOX5@LNP, SOX9@LNP, or SOX5/9@LNP (100 μL, 1 μg·mL^{-1}) via tail vein injection. Histopathological evaluation of major organs —including the heart, liver, spleen, lungs, and kidneys—was conducted by hematoxylin and eosin (H&E) staining. No

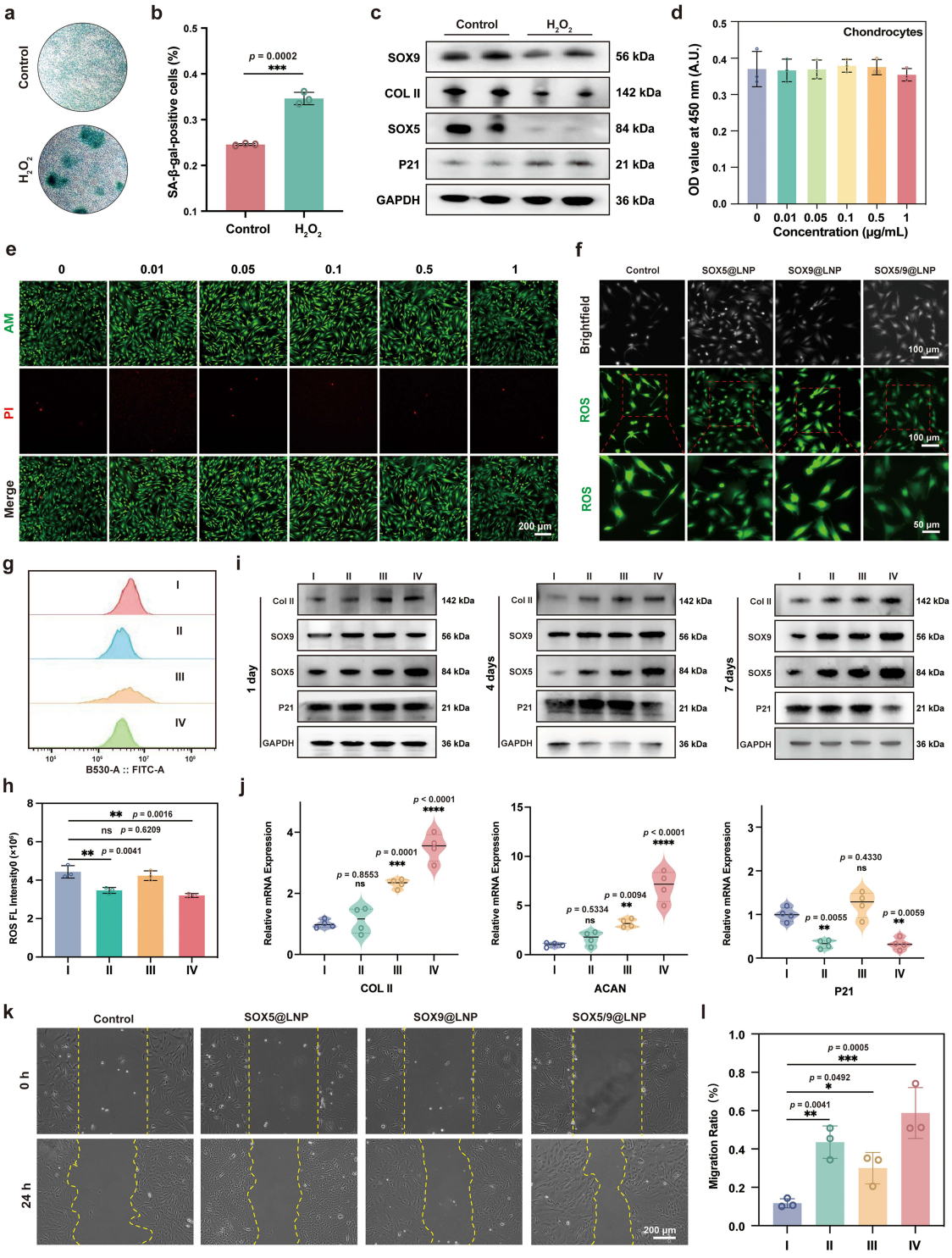

Figure 2 In vitro evaluation of SOX5/9@LNPs for reversing chondrocyte senescence and promoting cartilage regeneration. (**a**) Representative images of SA-β-Gal staining of chondrocytes after H_2O_2-induced senescence and control treatment. (**b**) Quantitative analysis of SA-β-Gal-positive cells. (**c**) Western blot analysis of SOX5, SOX9, COL II, P21, and GAPDH expression in normal and senescent chondrocytes. (**d**) Viability of chondrocytes after incubation with different concentrations of SOX5/9@LNPs, as assessed by CCK-8 assay (n = 3 for each group). (**e**) CLSM images of Calcein-AM/PI staining in chondrocytes treated with SOX5/9@LNPs at various concentrations. (**f**) CLSM images of intracellular ROS in chondrocytes under different treatment conditions. (**g**) Flow cytometry analysis of intracellular ROS levels in four treatment groups (control, SOX5@LNP, SOX9@LNP, SOX5/9@LNP). (**h**) Quantification of ROS levels, showing a significant decrease in the co-delivery group. (**i**) Representative Western blots showing time-dependent expression (days 1, 4, and 7) of COL II, SOX5, SOX9, and P21 after different treatments. (**j**) Relative mRNA levels of COL II, ACAN, and P21 at day 7 in chondrocytes treated with different LNPs, as determined by RT-qPCR. (**k** and **l**) Scratch wound healing assay and quantitative analysis of chondrocyte migration following treatment with Control, SOX5@LNP, SOX9@LNP, and SOX5/9@LNP. Yellow dashed lines indicate the wound edges at the initial and subsequent time points. Data are presented as mean ± SD, and statistical significance was determined by two-tailed *t*-test or ANOVA. Significance levels are indicated as follows: ns, not significant ($p > 0.05$); $^{*}p < 0.05$; $^{**}p < 0.01$; $^{***}p < 0.001$; $^{****}p < 0.0001$.

https://doi.org/10.2147/IJN.S544168

signs of tissue damage, necrosis, inflammation, or abnormal histological architecture were observed across all groups (Figure S5 in the ESM), further confirming the excellent in vivo biosafety of SOX5/9@LNPs. Importantly, no histological evidence of immune-related tissue injury or inflammatory cell infiltration was observed, further supporting the absence of immunotoxic effects in vivo. Routine hematological analysis revealed no significant alterations in red blood cell count (RBC), mean corpuscular volume (MCV), mean corpuscular hemoglobin (MCH), hematocrit (HCT), hemoglobin (HGB), platelet count (PLT), or white blood cell (WBC), lymphocyte (Lymph), monocyte (Mon) and granulocytes (Gran) parameters compared to the control group. Similarly, biochemical assessments of liver and kidney function, including alanine transaminase (ALT), aspartate transaminase (AST), alkaline phosphatase (ALP), blood urea nitrogen (BUN), and creatinine (CREA) levels, remained within normal ranges with no evidence of systemic toxicity (Figure S6 in the ESM). The stability of WBC counts, and differential subpopulations further indicates that systemic immune activation was not triggered by LNP administration.

Overall, these results clearly demonstrate that the SOX5/9@LNPs possess excellent biocompatibility both in vitro and in vivo. The absence of cytotoxicity, hematological abnormalities, biochemical disturbances, or histological damage strongly supports their translational potential as a safe and effective platform for mRNA-based therapy targeting osteoarthritic cartilage degeneration. Beyond these findings, our results are also consistent with the general advantages of ionizable lipid–based LNPs over conventional polymeric or non-ionizable lipid carriers. Ionizable LNPs promote efficient endosomal escape and transient cytoplasmic delivery of mRNA through pH-triggered protonation, which destabilizes endosomal membranes and induces non-lamellar phase transitions. This mechanism leads to higher and more predictable protein expression in vitro and in vivo, in line with previous studies showing that optimized ionizable LNPs achieve an excellent balance between efficacy and systemic tolerability.[29,54]

In vitro Evaluation of SOX5/9@LNP-Mediated Cartilage Regeneration and Senescence Alleviation

To examine the antioxidant and senescence-reversing potential of SOX5/9@LNPs, we first measured intracellular ROS levels in H_2O_2-induced senescent chondrocytes. Fluorescence imaging showed markedly reduced ROS accumulation in SOX5@LNP- and SOX5/9@LNP-treated cells, with the latter exhibiting the weakest signal, indicating the most effective suppression of oxidative stress (Figure 2f). Notably, cells treated with SOX5/9@LNP showed the weakest fluorescence signal among all groups, suggesting the most pronounced suppression of oxidative stress. To further substantiate these observations, flow cytometry analysis was performed to quantitatively assess intracellular ROS levels (Figure 2g). Subsequent statistical analysis (Figure 2h) demonstrated a significant reduction in ROS levels in the SOX5@LNP and SOX5/9@LNP groups, with the SOX5/9@LNP group achieving the most substantial decrease. In contrast, ROS levels in the SOX9@LNP group remained similar to those in the control. These results suggest that SOX5, particularly in combination with SOX9, plays a key role in alleviating oxidative stress in senescent chondrocytes, potentially contributing to the reversal of the senescence-associated phenotype.

To comprehensively evaluate the chondrogenic and anti-senescent effects of SOX5/9@LNPs, we performed a series of molecular and functional assays using hydrogen peroxide-induced senescent chondrocytes. These cells were treated with SOX5@LNP, SOX9@LNP, or a combination of both (SOX5/9@LNP) for 1, 4, and 7 days. Western blot analysis revealed dynamic temporal changes in protein expression (Figure 2i). Over the course of treatment, expression levels of cartilage-specific markers—including SOX5, SOX9, and type II collagen (COL II)—gradually increased, particularly in the SOX5/9@LNP group. In contrast, the senescence-associated protein p21 showed a progressive decrease in expression, with the most significant downregulation observed on day 7. Delivering SOX5 or SOX9 individually resulted in only slight increases in marker expression. However, when both were delivered together using LNPs, a much more significant effect was observed. This indicates a synergistic reversal of the senescent phenotype and a restoration of chondrocyte function. To further confirm these findings at the transcriptional level, RT-qPCR was performed to assess mRNA expression of COLII, aggrecan (ACAN), and p21 (Figure 2j). The results were in strong agreement with the protein data: COL II and ACAN mRNA levels were significantly upregulated following SOX5/9@LNP treatment, while p21 expression was markedly reduced. Notably, at all-time points the dual-treatment group outperformed the single-gene

groups, confirming that co-delivery of SOX5 and SOX9 more effectively stimulates the chondrogenic program while suppressing cellular aging signals. Mechanistically, the dual-TF configuration overcomes two failure modes of single-factor gene delivery—insufficient anabolic drive and incomplete senescence reversal—providing a rationale for the superior in-vivo protection observed subsequently. To evaluate the impact of SOX5/9@LNPs on chondrocyte motility, a scratch assay was conducted using senescent chondrocytes. As shown in Figure 2k, uniform scratches were introduced at 0 h across all groups. After 24 h, notable wound closure was observed in the SOX5/9@LNP-treated group, whereas wider gaps remained in the control, SOX5@LNP, and SOX9@LNP groups, indicating impaired migration. Quantitative analysis revealed that the average migration rate in the SOX5/9@LNP group reached nearly 60%, which was significantly higher than in all other groups (Figure 2L). These findings suggest that co-delivery of SOX5 and SOX9 can substantially enhance the migration capacity of senescent chondrocytes, facilitating functional recovery relevant to cartilage repair.

To further validate the rejuvenating effects of SOX5/9@LNPs on senescent chondrocytes, we conducted immunofluorescence analyses targeting extracellular matrix production, senescence markers, and mitochondrial function (Figure 3). Cells treated with SOX5/9@LNPs exhibited significantly elevated expression of cartilage-specific matrix proteins, COL II and aggrecan (ACAN), compared to both untreated and single-gene treated groups (Figure 3a and b). Consistently, JC-1 staining revealed a higher red-to-green fluorescence ratio in the SOX5/9@LNP group, indicating improved mitochondrial membrane potential and enhanced cellular metabolic activity (Figure 3c). In parallel, fluorescence signals of p21 and p16, two canonical senescence markers, were markedly diminished, indicating effective suppression of cellular aging pathways (Figure 3d and e). Given that mitochondrial dysfunction is a hallmark of senescence, this finding further substantiates the anti-aging efficacy of SOX5/9@LNP treatment at the organelle level. Collectively, these findings demonstrate that SOX5/9@LNP treatment rejuvenates senescent chondrocytes by restoring cartilage matrix production, dampening senescence-related signals, and improving mitochondrial function. This multifaceted approach underscores the high therapeutic potential of co-delivering SOX5 and SOX9 for cartilage regeneration in osteoarthritis. Following the demonstration of senescence alleviation in chondrocytes, the ability of SOX5/9@LNPs to drive chondrogenic differentiation in progenitor cells was further evaluated (Figure 3f). Rat bone marrow-derived mesenchymal stem cells (rBMSCs), known for their multilineage plasticity and relevance to cartilage tissue engineering,[55,56], were treated with SOX5/9@LNPs and evaluated at days 0, 1, 4, and 7 via Western blotting (Figure 3g) and immunofluorescence staining for type II collagen (COL II) expression (Figure 3h). Both analyses revealed a time-dependent upregulation of COL II protein, indicating successful activation of the chondrogenic transcriptional program and enhanced extracellular matrix synthesis.

Collectively, these data underscore that SOX5/9@LNPs not only reverse chondrocyte senescence but also effectively direct the lineage commitment of undifferentiated mesenchymal stem cells toward chondrogenesis. This dual functionality highlights the versatility of SOX5/9@LNPs as a cartilage-specific mRNA-based nanoplatform, capable of addressing key pathological features of osteoarthritis, including diminished cellular function, matrix loss, and impaired endogenous regeneration. These findings support the application of SOX5/9@LNPs as a promising disease-modifying therapeutic strategy for OA.

In vivo Evaluation of Cartilage Regeneration with SOX5/9@LNP Injection

To comprehensively assess the therapeutic efficacy of SOX5/9@LNPs in vivo, we employed a widely accepted anterior cruciate ligament transection (ACLT) model in Sprague–Dawley rats to simulate the progressive cartilage degradation characteristic of human OA (Figure 4). This model has been extensively used to mimic mechanical instability-induced OA-like changes, including cartilage erosion, synovial inflammation, and subchondral bone remodeling.[57–60] Two weeks post-surgery, intra-articular administration of SOX5@LNP, SOX9@LNP, or SOX5/9@LNP (1 μg mL^{-1}) was performed twice weekly for two consecutive weeks (Figure 4a). The sham-operated group, which did not undergo ACLT, served as the normal control, while the ACLT-only group (receiving intra-articular saline injections) was designated as the OA model control.

Animals were euthanized at the fourth and eighth postoperative weeks for comprehensive joint analysis. Micro-computed tomography (micro-CT) was utilized then to non-invasively assess structural changes in the subchondral bone

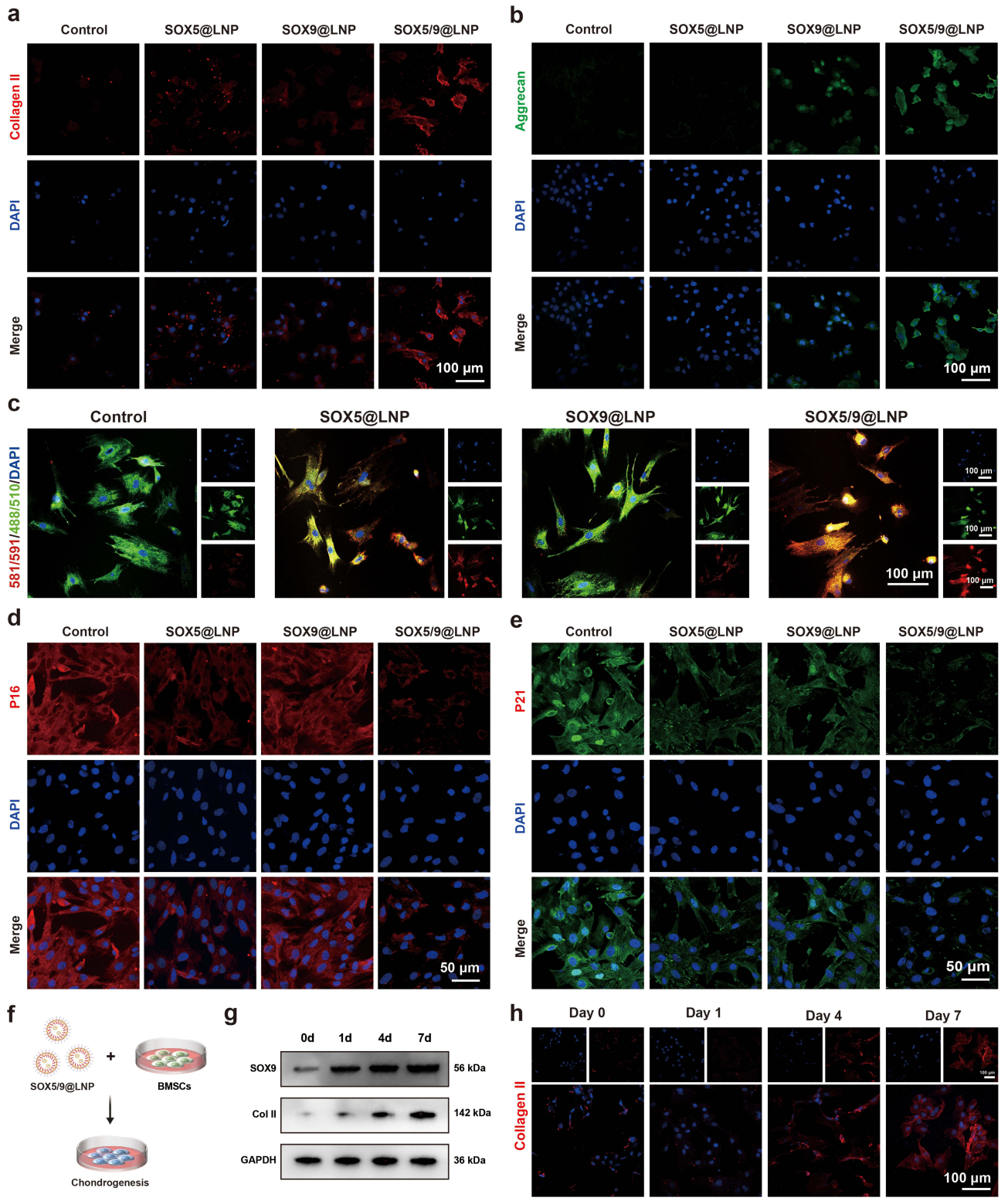

Figure 3 In vitro immunofluorescence and Western blot analyses validating SOX5/9@LNP-mediated chondrogenic induction and alleviation of chondrocyte senescence. (**a** and **b**) Immunofluorescences staining of collagen type II (COL II, red) and aggrecan (ACAN, green) in senescent chondrocytes after treatment with SOX5@LNP, SOX9@LNP and SOX5/9@LNP and nuclei were counterstained with DAPI (blue) (scale bar = 100 μm). (**c**) JC-1 staining images showing changes in mitochondrial membrane potential, with green fluorescence (monomers) and red fluorescence (aggregates) indicating mitochondrial integrity (scale bar = 100μm). (**d** and **e**) Immunofluorescence staining of senescence markers P16 (red) and P21 (green), respectively, in chondrocytes subjected to different treatments. DAPI (blue) was used for nuclear counterstaining (scale bar = 100 μm). (**f**) Schematic illustration of the co-culture system for investigating the chondrogenic potential of SOX5/9@LNP-treated rBMSCs. (**g** and **h**) Western blot and immunofluorescence analyses of COL II expression in rBMSCs treated with SOX5/9@LNPs for 0, 1, 4, and 7 days (scale bar = 100 μm).

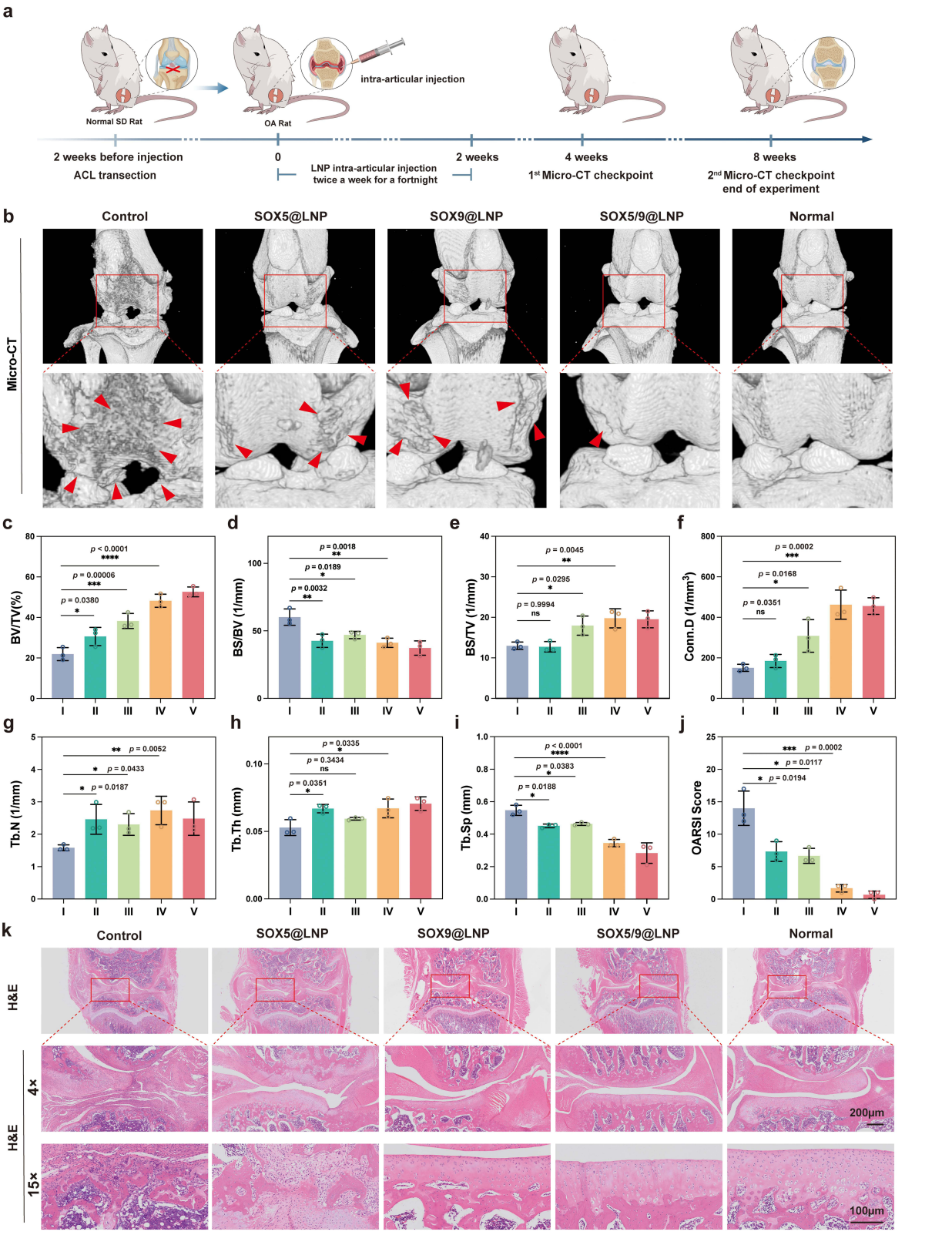

Figure 4 In vivo evaluation of SOX5/9@LNPs for cartilage regeneration in an ACLT-induced OA rat model. (**a**) Schematic illustration of the ACLT-induced osteoarthritis model and intra-articular LNP administration protocol. (**b**) Representative 3D micro-CT images in different groups after 8 weeks of treatment and red arrowheads indicate areas of cartilage erosion and osteophyte formation. Red arrowheads indicate areas of cartilage erosion and osteophyte formation. (**c–i**) Quantitative micro-CT assessments of structural parameters including bone volume fraction (BV/TV), bone surface–to–bone volume ratio (BS/BV), bone surface–to–tissue volume ratio (BS/TV), connectivity density (Conn.D), trabecular number (Tb.N), trabecular thickness (Tb.Th), and trabecular separation (Tb.Sp) across different treatment groups. (**j**) Quantitative OARSI histological scores in different groups after 8 weeks of treatment. (**k**) H&E staining images in different groups after treatment for 8 weeks. The statistical significance was calculated using a two-tailed *t* test. ns: not significant ($p > 0.05$); *$p < 0.05$; **$p < 0.01$; ***$p < 0.001$; ****$p < 0.0001$.

https://doi.org/10.2147/IJN.S544168

of the medial tibial plateau (Figures 4b, S7 and 8 in the ESM). In ACLT-induced osteoarthritic joints, typical pathological remodeling was evident, characterized by trabecular bone loss, reduced connectivity, and increased porosity. Quantitative analyses showed that the OA control group exhibited a significant reduction in bone volume fraction (BV/TV), tissue volume ratio (BS/TV) and connectivity density (Conn.D), accompanied by increases in bone volume ratio (BS/BV) and trabecular separation (Tb.Sp), as well as modest decreases in trabecular number (Tb.N) and thickness (Tb.Th). These changes are consistent with OA-associated bone resorption patterns (Figure 4c–i). In contrast, SOX5/9@LNP treatment effectively preserved subchondral bone microarchitecture. Three-dimensional reconstructions revealed denser and better-organized trabecular structures in the SOX5/9@LNP group, with significant increases in BV/TV, BS/TV, and Conn.D, as well as decreases in BS/BV and Tb.Sp. Modest increases in Tb.Th and Tb.N were also observed, whereas the reduction in Tb.Sp was statistically significant compared to both the OA control and the single-factor groups at 8 weeks ($p < 0.01$) (Figures 4c–i and S9 in the ESM). Importantly, while improvements at 4 weeks were already detectable, the differences became much more pronounced by 8 weeks, underscoring the time-dependent benefits of the dual-transcription factor therapy. In addition to summarizing time-dependent gains, these data indicate a mechanistic advantage over symptomatic intra-articular agents like glucocorticoids and hyaluronic acid, which seldom preserve subchondral microarchitecture. SOX5/9@LNPs not only maintained trabecular connectivity and reduced Tb.Sp alongside cartilage protection but also showed potential for modifying structure.[61] To further corroborate these observations, quantitative OARSI histological scoring was performed.[62] Consistent with the micro-CT findings, SOX5/9@LNP treatment resulted in significant reductions in cartilage degeneration scores by 8 weeks ($p < 0.001$), clearly outperforming both the OA control and single-gene treatment groups (Figures 4j and S9 in the ESM). Histological assessments paralleled these micro-CT findings. At 4 weeks, H&E staining demonstrated that SOX5/9@LNP-treated joints exhibited relatively smoother cartilage surfaces and improved cellular organization compared to the OA controls, albeit with some residual surface irregularities (Figure S10 in the ESM). The initial, albeit modest improvements observed at 4 weeks are likely due to the rapid transcriptional reprogramming of senescent chondrocytes. In contrast, the more significant gains seen at 8 weeks are consistent with the accumulation of newly synthesized extracellular matrix driven by the SOX5/SOX9 axis. By 8 weeks, these protective effects became markedly accentuated: the SOX5/9@LNP group maintained an intact cartilage surface, organized chondrocyte columns, and robust matrix integrity, whereas severe erosion and matrix loss dominated the OA control joints (Figure 4k). Masson's trichrome staining confirmed better collagen fiber continuity (Figure 5a), and Safranin O/Fast Green and Toluidine Blue staining revealed more pronounced retention of glycosaminoglycans (GAGs) in the SOX5/9@LNP group (Figure 5b and c). Immunohistochemical staining for type II collagen (COL II) further demonstrated uniform and strong matrix protein expression, consistent with active chondrogenic remodeling (Figure 5d). Notably, staining at 4 weeks (Figure S11 in the ESM) also showed trends of improvement, though the differences were less pronounced than those observed at 8 weeks. Preservation of GAGs (Safranin O) alongside uniform type II collagen deposition is considered indicative of hyaline-like cartilage matrix according to ICRS histologic criteria.[63,64] Novel approaches, such as hydrogel/organoid constructs and bone-targeted nanoparticles, have been investigated for reconstructing cartilage microenvironments or regulating subchondral remodeling, but these methods typically rely on scaffolds or chemical targeting.[19,20,65] In contrast, our SOX5/9@LNPs work by reprogramming chondrocytes in situ through transient mRNA delivery, which results in the restoration of matrix synthesis without the need for external implants or permanent modifications. Current intra-articular glucocorticoids and hyaluronic acid, on the other hand, are primarily used for symptom relief rather than structural modification. Zonal restoration is usually pursued using engineered multizonal scaffolds or organoid/hydrogel systems.[66] Taken together, these results suggest that while early therapeutic benefits were detectable, the dual-transcription factor strategy mediated progressively enhanced cartilage protection and regeneration with prolonged treatment duration. Consistently, the transient co-expression of two master transcription factors through mRNA leads to better functional rescue compared to delivering a single factor alone. This approach also avoids genomic integration, which aligns with the superior histology and micro-CT results seen in this study.

In summary, intra-articular administration of SOX5/9@LNPs significantly enhanced cartilage integrity, preserved subchondral bone architecture, and attenuated osteoarthritic degeneration during both early and intermediate stages following joint injury. The integrated molecular and histological findings underscore the therapeutic efficacy of SOX5

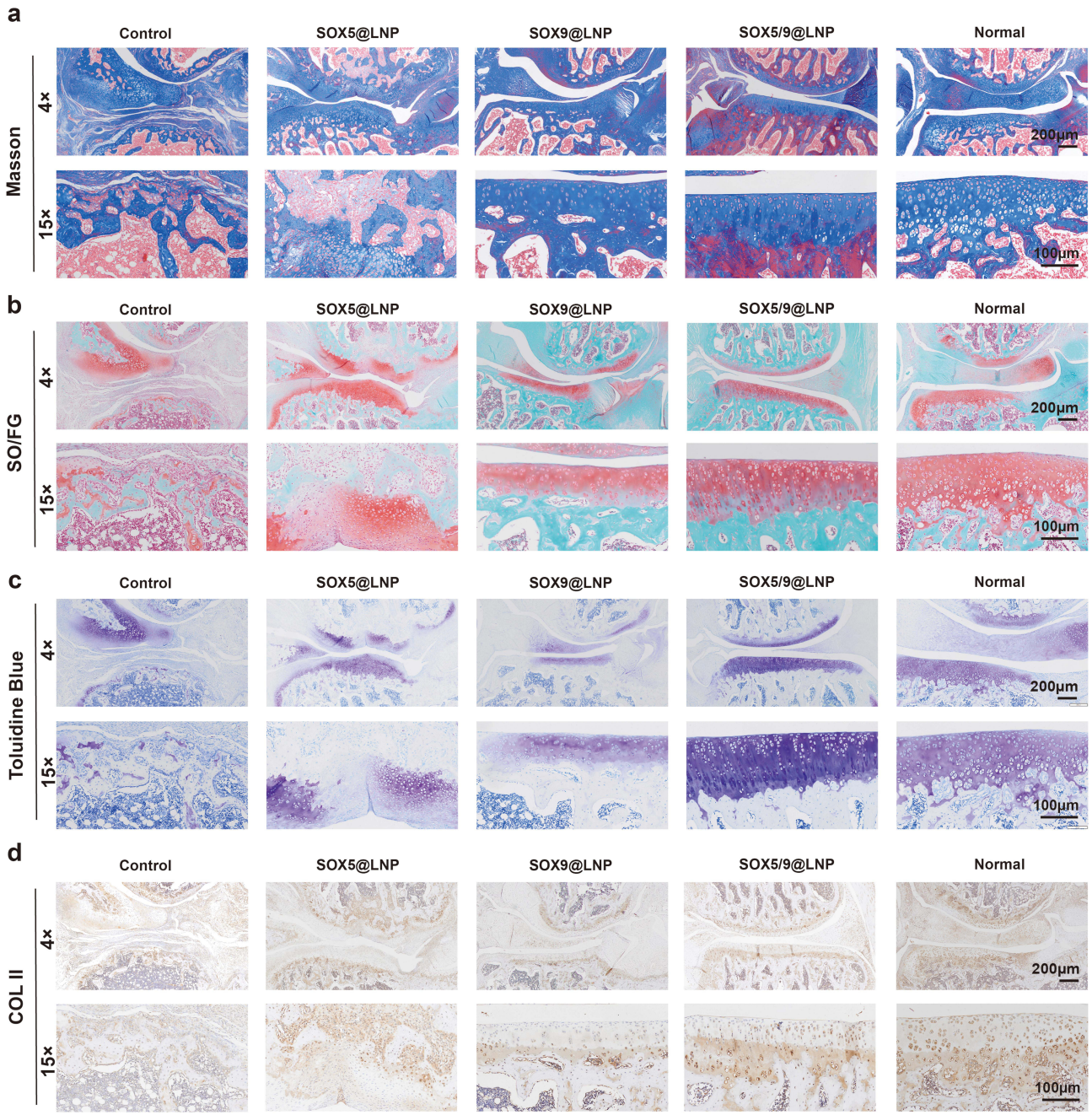

Figure 5 Histological and immunohistochemical evaluation of cartilage repair. (**a**) Masson's trichrome staining showing collagen fiber distribution and organization in cartilage tissues. (**b**) SO-FG staining demonstrating proteoglycan content in the extracellular matrix. (**c**) Toluidine blue staining showing sulfated glycosaminoglycan distribution. (**d**) Immunohistochemical staining of collagen type II (COL II) indicating the extent of cartilage matrix restoration. The SOX5/9@LNP group showed superior ECM restoration and cartilage regeneration compared to other treatment groups.

and SOX9 mRNA co-delivery and highlight this strategy as a compelling and disease-modifying approach for in vivo cartilage regeneration in osteoarthritis. Moving forward, our translational efforts will prioritize the definition of dosing intervals and the evaluation of sustained benefits beyond 8 weeks in load-bearing large-animal joints. This will be complemented by a thorough analysis of long-term biodistribution, immunogenicity, and potential off-target effects. To enhance intra-articular retention and tissue penetration, we will explore the use of cartilage-affinity or matrix-binding ligands. Moreover, we will carry out repeat-dose studies with gait and functional assessments, while advancing the

development of Good Manufacturing Practice (GMP)-consistent formulation and release testing to facilitate clinical translation.

RNA Sequence Analysis

To assess the therapeutic potential of SOX5/9@LNPs in OA, RNA sequencing was performed on chondrocytes from treated and untreated OA groups. Differential expression analysis revealed a substantial transcriptomic shift, with 487 genes significantly upregulated ($|\log_2 FC| > 1$, p-adjusted < 0.05). Notably, several stress- and metabolism-associated genes, including Sod2, Gbe1, Car9, and Pgk1, were highly upregulated under IL1B stimulation but substantially downregulated upon SOX5/9@LNP treatment, suggesting that the intervention mitigated the inflammatory and oxidative stress responses rather than simply activating these pathways (Figure 6a and b). Among these, Sod2, a mitochondrial superoxide dismutase, is pivotal in neutralizing reactive oxygen species (ROS), thereby mitigating oxidative stress-induced senescence.[67,68] In parallel, the upregulation of Mmp3, a key matrix metalloproteinase, suggests active initiation of ECM remodeling processes.[69] Functional enrichment analysis further demonstrated that these differentially expressed genes were significantly associated with pathways related to extracellular matrix organization, angiogenesis, ECM-receptor interaction, and MAPK signaling—all of which are critical for cartilage homeostasis and repair. These findings suggest that SOX5/9@LNP exerts a dual mechanism of action: on one hand, reversing chondrocyte senescence by reactivating antioxidant and metabolic pathways; on the other hand, promoting cartilage regeneration by stimulating ECM synthesis and activating reparative signaling. Enrichment of GO and KEGG terms related to developmental and stress-responsive processes reinforces the hypothesis that SOX5/9 mRNA delivery reprograms senescent chondrocytes toward a regenerative phenotype (Figure 6c and d).

To further elucidate the underlying regulatory networks, a protein–protein interaction (PPI) analysis based on the STRING database was conducted. A total of 116 high-confidence interaction pairs (score > 700) were identified, involving cartilage-specific and aging-related genes such as SOX9, SOX5, COL2A1, ACAN, MMP3, P21, and SOD2. Dense network clustering around SOX9 and COL2A1 highlighted their central role in matrix synthesis, while stress-related nodes including SOD2 and P21 were closely linked with inflammatory mediators such as NOS3, C3, and CXCL5, underscoring the interplay between senescence, inflammation, and cartilage degeneration (Figure 6e). To validate the activation of key signaling pathways at the protein level, we conducted Western blot analysis of core components of the MAPK pathway, including ERK, JNK, and p38, along with their phosphorylated forms. The results revealed significantly increased levels of p-ERK, p-JNK, and p-p38 in the SOX5/9@LNP-treated group, indicating activation of MAPK signaling cascades (Figure 6f). These findings are consistent with the KEGG enrichment results and provide further mechanistic support for the involvement of MAPK-driven stress response and regenerative signaling in SOX5/9@LNP-mediated cartilage repair.

Finally, to further validate the transcriptomic impact of SOX5/9@LNP treatment, we compared gene expression profiles between the SOX5/9@LNP- treated group and normal group (Figure S12 in the ESM). Only moderate transcriptomic alterations were observed, with few significantly differentially expressed genes. Clustering analyses revealed normalization of inflammation- and senescence-related transcripts (eg, Cdkn1a, Nos2, Ccl5), while GO enrichment highlighted restoration of pathways associated with cell cycle and mitotic spindle organization. These data suggest that SOX5/9@LNPs partially reprogram OA chondrocytes toward a more proliferative, regenerative state without inducing off-target or global transcriptional dysregulation.

Conclusions

In summary, we developed a dual-functional mRNA nanotherapeutic platform for osteoarthritis (OA) by co-delivering SOX5 and SOX9 via rationally optimized SM-102-based lipid nanoparticles (SOX5/9@LNP). This system simultaneously targets cartilage regeneration and subchondral bone preservation. In vitro, SOX5/9@LNP effectively reversed chondrocyte senescence, enhanced extracellular matrix synthesis, and promoted chondrogenic differentiation of bone marrow-derived mesenchymal stem cells, outperforming single-factor delivery. In vivo, intra-articular administration of SOX5/9@LNPs in an ACLT-induced OA rat model significantly preserved cartilage architecture and subchondral bone integrity, as evidenced by micro-CT analysis, histological staining, and OARSI scoring. With excellent biosafety and

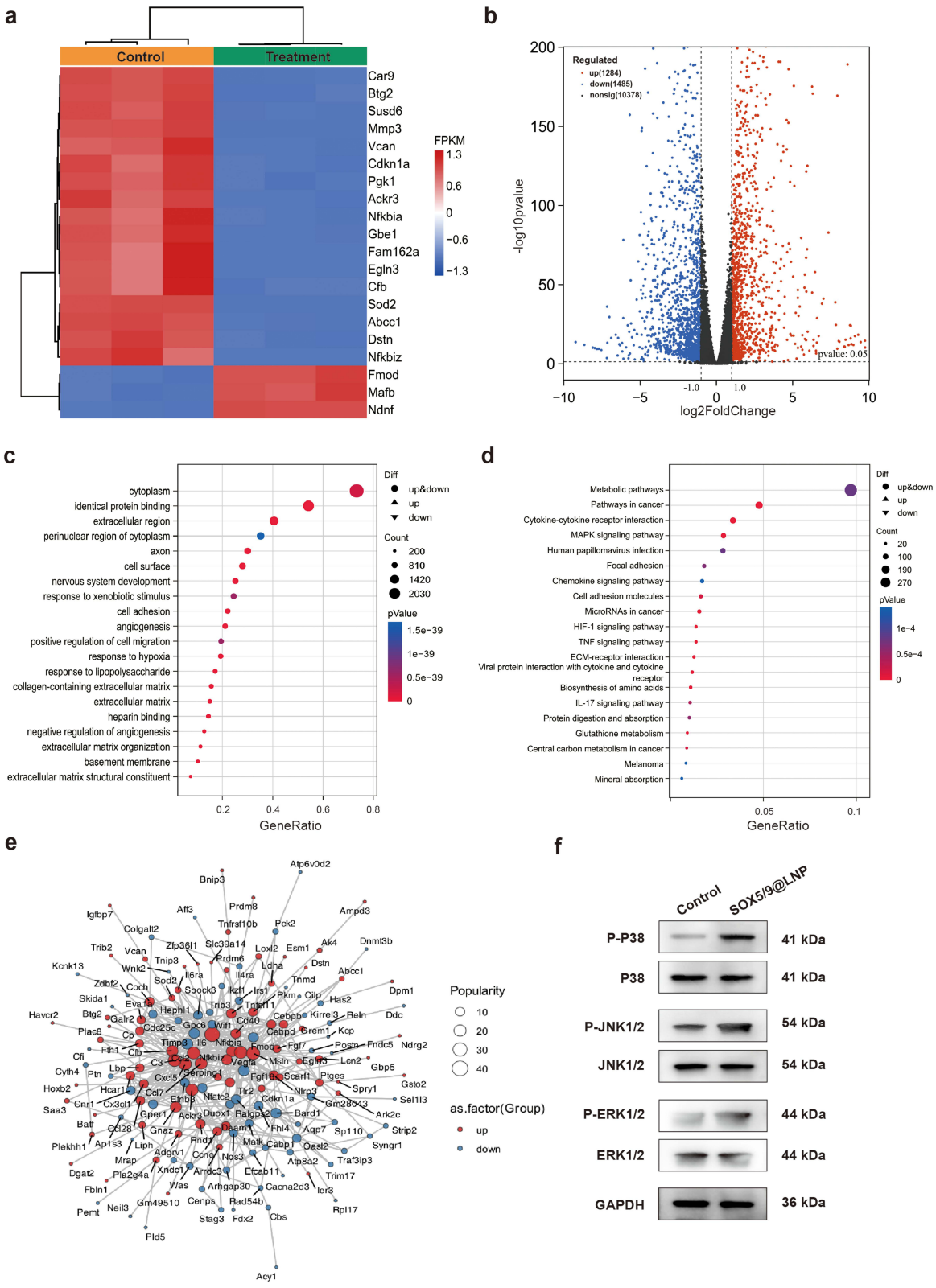

Figure 6 Transcriptomic analysis of SOX5/9@LNP treatment on senescent chondrocytes. (**a**) Heatmap of differentially expressed genes between the control and SOX5/9@LNP-treated groups, showing distinct expression profiles. (**b**) Volcano plot displaying significantly upregulated (red) and downregulated (blue) genes ($|\log_2 FC| > 1$, p-adjusted < 0.05). (**c**) Gene Ontology (GO) enrichment analysis of upregulated genes after SOX5/9@LNP treatment. (**d**) KEGG pathway enrichment analysis showing the most enriched signaling pathways, including MAPK and PI3K-Akt signaling. (**e**) Protein–protein interaction (PPI) network of differentially expressed genes highlighting key nodes associated with cartilage homeostasis and senescence. (**f**) Western blot analysis of MAPK signaling pathway components (ERK1/2, JNK1/2, and p38) and their phosphorylated forms, validating transcriptomic findings.

https://doi.org/10.2147/IJN.S544168

potent regenerative effects, this strategy represents a promising disease-modifying approach for OA. Beyond offering mechanistic insights into senescence reversal and matrix restoration, our study also expands the therapeutic scope of mRNA-loaded lipid nanocarriers in orthopedic regenerative medicine.

Abbreviations

OA, osteoarthritis; NSAIDs, nonsteroidal anti-inflammatory drugs; ECM, extracellular matrix; PRP, platelet-rich plasma; SA-β-Gal, senescence-associated β-galactosidase; LNPs, lipid nanoparticles; rBMSCs, rat bone marrow-derived mesenchymal stem cells; SASP, senescence-associated secretory phenotype; mRNA, messenger RNA; COL2, type II collagen; ACAN, aggrecan; TEM, Transmission electron microscopy; PDI, polydispersity index; DLS, Dynamic light scattering; ROS, reactive oxygen species; ACLT, anterior cruciate ligament transection; DMEM, Dulbecco's Modified Eagle Medium; FBS, fetal bovine serum; PBS, phosphate-buffered saline; ANOVA, analysis of variance; CLSM, confocal laser scanning microscope.

Data Sharing Statement

All data generated or analysed during this study are included in this article.

Acknowledgments

We would like to express our sincere gratitude to Professor Yuhong Cao (CAS Key Laboratory for Biological Effects of Nanomaterials and Nanosafety, National Center for Nanoscience and Technology, Chinese Academy of Sciences) for her valuable academic guidance and insightful discussions during the conceptualization and design of this study.

Author Contributions

All authors made a significant contribution to the work reported, whether that is in the conception, study design, execution, acquisition of data, analysis and interpretation, or in all these areas; took part in drafting, revising or critically reviewing the article; gave final approval of the version to be published; have agreed on the journal to which the article has been submitted; and agree to be accountable for all aspects of the work.

Funding

This work was financially supported by the National Natural Science Foundation of China (Grant No. 82372410 and 81972046) and the National High Level Hospital Clinical Research Funding (Grant number: 2022-PUMCH-B-001).

Disclosure

The authors report no conflicts of interest in this work.

References

1. Cross M, Smith E, Hoy D, et al. The global burden of hip and knee osteoarthritis: estimates from the global burden of disease 2010 study. *Ann Rheum Dis*. 2014;73(7):1323–1330. doi:10.1136/annrheumdis-2013-204763
2. Glyn-Jones S, Palmer AJ, Agricola R, et al. Osteoarthritis. *Lancet*. 2015;386(9991):376–387. doi:10.1016/s0140-6736(14)60802-3
3. Tong L, Yu H, Huang X, et al. Current understanding of osteoarthritis pathogenesis and relevant new approaches. *Bone Res*. 2022;10(1):60. doi:10.1038/s41413-022-00226-9
4. Yao Q, Wu X, Tao C, et al. Osteoarthritis: pathogenic signaling pathways and therapeutic targets. *Signal Transduct Target Ther*. 2023;8(1):56. doi:10.1038/s41392-023-01330-w
5. Chen D, Shen J, Zhao W, et al. Osteoarthritis: toward a comprehensive understanding of pathological mechanism. *Bone Res*. 2017;5(1):16044. doi:10.1038/boneres.2016.44
6. Barnett R. Osteoarthritis. *Lancet*. 2018;391(10134):1985. doi:10.1016/s0140-6736(18)31064-x
7. Martel-Pelletier J, Barr AJ, Cicuttini FM, et al. Osteoarthritis. *Nat Rev Dis Primers*. 2016;2:16072. doi:10.1038/nrdp.2016.72
8. He Y, Li Z, Alexander PG, et al. Pathogenesis of osteoarthritis: risk factors, regulatory pathways in chondrocytes, and experimental models. *Biology*. 2020;9(8):194. doi:10.3390/biology9080194
9. Hunter DJ, Bierma-Zeinstra S. Osteoarthritis. *Lancet*. 2019;393(10182):1745–1759. doi:10.1016/s0140-6736(19)30417-9
10. Scheuing WJ, Reginato AM, Deeb M, Acer Kasman S. The burden of osteoarthritis: is it a rising problem? *Best Pract Res Clin Rheumatol*. 2023;37(2):101836. doi:10.1016/j.berh.2023.101836

11. Ma W, Chen H, Yuan Q, Chen X, Li H. Global, regional, and national epidemiology of osteoarthritis in working-age individuals: insights from the global burden of disease study 1990–2021. *Scientific Reports*. 2025;15(1):7907. doi:10.1038/s41598-025-91783-6
12. DeJulius CR, Walton BL, Colazo JM, et al. Engineering approaches for RNA-based and cell-based osteoarthritis therapies. *Nat Rev Rheumatol*. 2024;20(2):81–100. doi:10.1038/s41584-023-01067-4
13. Hu S, Zhang C, Ni L, et al. Stabilization of HIF-1α alleviates osteoarthritis via enhancing mitophagy. *Cell Death Dis*. 2020;11(6):481. doi:10.1038/s41419-020-2680-0
14. Hunter DJ, March L, Chew M. Osteoarthritis in 2020 and beyond: a lancet commission. *Lancet*. 2020;396(10264):1711–1712. doi:10.1016/s0140-6736(20)32230-3
15. Calders P, Van Ginckel A. Presence of comorbidities and prognosis of clinical symptoms in knee and/or hip osteoarthritis: a systematic review and meta-analysis. *Semin Arthritis Rheum*. 2018;47(6):805–813. doi:10.1016/j.semarthrit.2017.10.016
16. Baker DJ, Wijshake T, Tchkonia T, et al. Clearance of p16Ink4a-positive senescent cells delays ageing-associated disorders. *Nature*. 2011;479(7372):232–236. doi:10.1038/nature10600
17. Loeser RF. Aging and osteoarthritis: the role of chondrocyte senescence and aging changes in the cartilage matrix. *Osteoarthritis Cartilage*. 2009;17(8):971–979. doi:10.1016/j.joca.2009.03.002
18. Migliore A, Paoletta M, Moretti A, Liguori S, Iolascon G. The perspectives of intra-articular therapy in the management of osteoarthritis. *Expert Opin Drug Deliv*. 2020;17(9):1213–1226. doi:10.1080/17425247.2020.1783234
19. Shen C, Zhou Z, Li R, et al. Silk fibroin-based hydrogels for cartilage organoids in osteoarthritis treatment. *Theranostics*. 2025;15(2):560–584. doi:10.7150/thno.103491
20. Li X, Sheng S, Li G, et al. Research progress in hydrogels for cartilage organoids. *Adv Healthc Mater*. 2024;13(22):e2400431. doi:10.1002/adhm.202400431
21. Jeon OH, Kim C, Laberge R-M, et al. Local clearance of senescent cells attenuates the development of post-traumatic osteoarthritis and creates a pro-regenerative environment. *Nature Medicine*. 2017;23(6):775–781. doi:10.1038/nm.4324
22. Shi Y, Shi M, Wang Y, You J. Progress and prospects of mRNA-based drugs in pre-clinical and clinical applications. *Signal Transduct Target Ther*. 2024;9(1):322. doi:10.1038/s41392-024-02002-z
23. Li X, Qiu W, Li J, et al. First-generation species-selective chemical probes for fluorescence imaging of human senescence-associated β-galactosidase. *Chem Sci*. 2020;11(28):7292–7301. doi:10.1039/d0sc01234c
24. Jeon OH, David N, Campisi J, Elisseeff JH. Senescent cells and osteoarthritis: a painful connection. *J Clin Invest*. 2018;128(4):1229–1237. doi:10.1172/jci95147
25. Gao SG, Zeng C, Li LJ, et al. Correlation between senescence-associated beta-galactosidase expression in articular cartilage and disease severity of patients with knee osteoarthritis. *Int J Rheum Dis*. 2016;19(3):226–232. doi:10.1111/1756-185x.12096
26. Xu M, Bradley EW, Weivoda MM, et al. Transplanted senescent cells induce an osteoarthritis-like condition in mice. *J Gerontol a Biol Sci Med Sci*. 2017;72(6):780–785. doi:10.1093/gerona/glw154
27. Atasoy-Zeybek A, Showel KK, Nagelli CV, Westendorf JJ, Evans CH. The intersection of aging and estrogen in osteoarthritis. *NPJ Womens Health*. 2025;3(1):15. doi:10.1038/s44294-025-00063-1
28. Diekman BO, Loeser RF. Aging and the emerging role of cellular senescence in osteoarthritis. *Osteoarthritis Cartilage*. 2024;32(4):365–371. doi:10.1016/j.joca.2023.11.018
29. Hou X, Zaks T, Langer R, Dong Y. Lipid nanoparticles for mRNA delivery. *Nat Rev Mater*. 2021;6(12):1078–1094. doi:10.1038/s41578-021-00358-0
30. Huang X, Kong N, Zhang X, Cao Y, Langer R, Tao W. The landscape of mRNA nanomedicine. *Nat Med*. 2022;28(11):2273–2287. doi:10.1038/s41591-022-02061-1
31. Pardi N, Hogan MJ, Porter FW, Weissman D. mRNA vaccines - a new era in vaccinology. *Nat Rev Drug Discov*. 2018;17(4):261–279. doi:10.1038/nrd.2017.243
32. Sahin U, Muik A, Derhovanessian E, et al. COVID-19 vaccine BNT162b1 elicits human antibody and T(H)1 T cell responses. *Nature*. 2020;586(7830):594–599. doi:10.1038/s41586-020-2814-7
33. Verbeke R, Lentacker I, De Smedt SC, Dewitte H. Three decades of messenger RNA vaccine development. *Nano Today*. 2019;28:100766. doi:10.1016/j.nantod.2019.100766
34. Sahin U, Karikó K, Türeci Ö. mRNA-based therapeutics--developing a new class of drugs. *Nat Rev Drug Discov*. 2014;13(10):759–780. doi:10.1038/nrd4278
35. Zhu Y, Zhu L, Wang X, Jin H. RNA-based therapeutics: an overview and prospectus. *Cell Death Dis*. 2022;13(7):644. doi:10.1038/s41419-022-05075-2
36. Zhao DW, Zhang J, Chen C, et al. Rejuvenation modulation of nucleus pulposus progenitor cells reverses senescence-associated intervertebral disc degeneration. *Adv Mater*. 2025;37(7):e2409979. doi:10.1002/adma.202409979
37. Oguma T, Kanazawa T, Kaneko YK, et al. Effects of phospholipid type and particle size on lipid nanoparticle distribution in vivo and in pancreatic islets. *J Control Release*. 2024;373:917–928. doi:10.1016/j.jconrel.2024.07.059
38. Miao L, Zhang Y, Huang L. mRNA vaccine for cancer immunotherapy. *Mol Cancer*. 2021;20(1):41. doi:10.1186/s12943-021-01335-5
39. Kon E, Ad-El N, Hazan-Halevy I, Stotsky-Oterin L, Peer D. Targeting cancer with mRNA-lipid nanoparticles: key considerations and future prospects. *Nat Rev Clin Oncol*. 2023;20(11):739–754. doi:10.1038/s41571-023-00811-9
40. Neefjes M, van Caam APM, van der Kraan PM. Transcription factors in cartilage homeostasis and osteoarthritis. *Biology*. 2020;9(9):290. doi:10.3390/biology9090290
41. Zuo C, Wang L, Kamalesh RM, et al. SHP2 regulates skeletal cell fate by modifying SOX9 expression and transcriptional activity. *Bone Res*. 2018;6:12. doi:10.1038/s41413-018-0013-z
42. Gadomski SJ, Mui BWH, Gorodetsky R, et al. Time- and cell-specific activation of BMP signaling restrains chondrocyte hypertrophy. *iScience*. 2024;27(8):110537. doi:10.1016/j.isci.2024.110537
43. Zhang X, Wu S, Zhu Y, Chu CQ. Exploiting joint-resident stem cells by exogenous SOX9 for cartilage regeneration for therapy of osteoarthritis. *Front Med*. 2021;8:622609. doi:10.3389/fmed.2021.622609

44. Chang SH, Mori D, Kobayashi H, et al. Excessive mechanical loading promotes osteoarthritis through the gremlin-1-NF-κB pathway. *Nat Commun*. 2019;10(1):1442. doi:10.1038/s41467-019-09491-5
45. Zhao L, Lai Y, Jiao H, Li J, Lu K, Huang J. CRISPR-mediated Sox9 activation and RelA inhibition enhance cell therapy for osteoarthritis. *Mol Ther*. 2024;32(8):2549–2562. doi:10.1016/j.ymthe.2024.06.016
46. Hattori T, Coustry F, Stephens S, et al. Transcriptional regulation of chondrogenesis by coactivator Tip60 via chromatin association with Sox9 and Sox5. *Nucleic Acids Res*. 2008;36(9):3011–3024. doi:10.1093/nar/gkn150
47. Liu CF, Lefebvre V. The transcription factors SOX9 and SOX5/SOX6 cooperate genome-wide through super-enhancers to drive chondrogenesis. *Nucleic Acids Res*. 2015;43(17):8183–8203. doi:10.1093/nar/gkv688
48. Song H, Park KH. Regulation and function of SOX9 during cartilage development and regeneration. *Semin Cancer Biol*. 2020;67(Pt 1):12–23. doi:10.1016/j.semcancer.2020.04.008
49. Lefebvre V, Behringer RR, de Crombrugghe B. L-Sox5, Sox6 and Sox9 control essential steps of the chondrocyte differentiation pathway. *Osteoarthritis Cartilage*. 2001;9(Suppl A):S69–75. doi:10.1053/joca.2001.0447
50. Jing Y, Jiang X, Ji Q, et al. Genome-wide CRISPR activation screening in senescent cells reveals SOX5 as a driver and therapeutic target of rejuvenation. *Cell Stem Cell*. 2023;30(11):1452–1471.e10. doi:10.1016/j.stem.2023.09.007
51. Shah A, Aftab S, Nisar J, Ashiq MN, Iftikhar FJ. Nanocarriers for targeted drug delivery. *J Drug Deliv Sci Technol*. 2021;62:102426. doi:10.1016/j.jddst.2021.102426
52. Wang X, Li L, Li L, Song F, Song F. Interplay of nanoparticle properties during endocytosis. *Crystals*. 2021;11(7):728. doi:10.3390/cryst11070728
53. Zhang S, Li J, Lykotrafitis G, Bao G, Suresh S. Size-dependent endocytosis of nanoparticles. *Adv Mater*. 2009;21:419–424. doi:10.1002/adma.200801393
54. Ren Y, Lin L, Abdallah M, et al. Impact of ionizable lipid type on the pharmacokinetics and biodistribution of mRNA-lipid nanoparticles after intravenous and subcutaneous injection. *J Control Release*. 2025;384:113945. doi:10.1016/j.jconrel.2025.113945
55. Yang C, Chen R, Chen C, et al. Tissue engineering strategies hold promise for the repair of articular cartilage injury. *Biomed Eng Online*. 2024;23(1):92. doi:10.1186/s12938-024-01260-w
56. Fafián-Labora J, Fernández-Pernas P, Fuentes I, et al. Influence of age on rat bone-marrow mesenchymal stem cells potential. *Scientific Reports*. 2015;5(1):16765. doi:10.1038/srep16765
57. Liu L, Zhang W, Liu T, et al. The physiological metabolite α-ketoglutarate ameliorates osteoarthritis by regulating mitophagy and oxidative stress. *Redox Biol*. 2023;62:102663. doi:10.1016/j.redox.2023.102663
58. Zou Z, Hu W, Kang F, et al. Interplay between lipid dysregulation and ferroptosis in chondrocytes and the targeted therapy effect of metformin on osteoarthritis. *J Adv Res*. 2025;69:515–529. doi:10.1016/j.jare.2024.04.012
59. Lu H, Wei J, Liu K, et al. Radical-scavenging and subchondral bone-regenerating nanomedicine for osteoarthritis treatment. *ACS Nano*. 2023;17(6):6131–6146. doi:10.1021/acsnano.3c01789
60. Li K, Yan G, Huang H, et al. Anti-inflammatory and immunomodulatory effects of the extracellular vesicles derived from human umbilical cord mesenchymal stem cells on osteoarthritis via M2 macrophages. *J Nanobiotechnology*. 2022;20(1):38. doi:10.1186/s12951-021-01236-1
61. McAlindon TE, LaValley MP, Harvey WF, et al. Effect of intra-articular triamcinolone vs saline on knee cartilage volume and pain in patients with knee osteoarthritis: a randomized clinical trial. *JAMA*. 2017;317(19):1967–1975. doi:10.1001/jama.2017.5283
62. Gerwin N, Bendele AM, Glasson S, Carlson CS. The OARSI histopathology initiative - recommendations for histological assessments of osteoarthritis in the rat. *Osteoarthritis Cartilage*. 2010;18 (Suppl 3):S24–34. doi:10.1016/j.joca.2010.05.030
63. Hoemann C, Kandel R, Roberts S, et al. International Cartilage Repair Society (ICRS) recommended guidelines for histological endpoints for cartilage repair studies in animal models and clinical trials. *Cartilage*. 2011;2(2):153–172. doi:10.1177/1947603510397535
64. Mainil-Varlet P, Van Damme B, Nesic D, Knutsen G, Kandel R, Roberts S. A new histology scoring system for the assessment of the quality of human cartilage repair: ICRS II. *Am J Sports Med*. 2010;38(5):880–890. doi:10.1177/0363546509359068
65. Geng Z, Wang X, Yu Y, Ji L, Wang J, Liu C. Attenuating osteoarthritis by a high efficient anti-bone resorption injectable pH-responsive bisphosphonate-conjugated nano-apatite system. *Chem Eng J*. 2021;420:127674. doi:10.1016/j.cej.2020.127674
66. Lin X, Zhang Y, Li J, et al. Biomimetic multizonal scaffolds for the reconstruction of zonal articular cartilage in chondral and osteochondral defects. *Bioact Mater*. 2025;43:510–549. doi:10.1016/j.bioactmat.2024.10.001
67. Velarde MC, Flynn JM, Day NU, Melov S, Campisi J. Mitochondrial oxidative stress caused by Sod2 deficiency promotes cellular senescence and aging phenotypes in the skin. *Aging*. 2012;4(1):3–12. doi:10.18632/aging.100423
68. Wang Y, Branicky R, Noë A, Hekimi S. Superoxide dismutases: dual roles in controlling ROS damage and regulating ROS signaling. *J Cell Biol*. 2018;217(6):1915–1928. doi:10.1083/jcb.201708007
69. Wan J, Zhang G, Li X, et al. Matrix metalloproteinase 3: a promoting and destabilizing factor in the pathogenesis of disease and cell differentiation. *Front Physiol*. 2021;12:663978. doi:10.3389/fphys.2021.663978